Where the Red Chert Grows:
An investigation into a potential source of red clasts glacially distributed throughout the Puget Lowland

Derek J-A. Beal

A report prepared in partial fulfillment of the requirements for the degree of

Master of Science
Applied Geosciences

University of Washington

December 2016

Project mentor:
Dr. Eric Cheney

Project coordinator:
Kathy Troost

Reading committee:
Dr. Charlotte Schreiber
Dr. Darrel Cowan

MESSAGe Technical Report Number: 043

ABSTRACT

Clasts of fine grained siliceous red rock or red clasts (RC) have been found on many beaches around Puget Sound, Washington by E. Cheney from the University of Washington. Cheney plotted the locations of RC and created an isoline map showing concentrations of larger RC in the Whidbey Island area. Because of the abundance of larger clasts within Puget Sound and the glacial history within the region, a likely source of RC may be located in the southwestern Cascades. Red rocks very similar to what is observed on Puget Sound beaches is described in the Canyon Creek Unit by Vance (1957) located near Verlot, WA, directly east of Whidbey Island. Thin sections of the beach cobbles obtained by Cheney were compared with thin sections from the Canyon Creek Unit to determine if it could be identified as a source of RC. Although there are many similarities between the beach cobbles and the Canyon Creek Unit, it can only be considered a plausible source for RC found on Puget Sound beaches given the amount of data collected. A more intense sampling campaign of both sources along with additional analysis methods are required to fully confirm, or deny the Canyon Creek as a source of the RC within the Puget Lowland.

©2016 by Derek J-A. Beal
All Rights Reserved

CONTENTS

LIST OF FIGURES

LIST OF TABLES

ACKNOWLEDGEMENTS

This project could have not been completed without the help and advice from many exemplary individuals. I would like to thank Dr. Eric Cheney for the project idea and his continued help and advice. I would also like to thank Dr. Darrel Cowan, Dr. Charlotte Schreiber, Dr. Juliet Crider, and Kathy Troost for their ongoing words of wisdom, encouragement, and most importantly their patience with me. Jim Miller, Patrick Kao, and Ross Logan were crucial and inspirational during many difficult field campaigns. And last, but not at all least I would like to thank Kristin Beck for her motivational support and overall awesomeness.

INTRODUCTION

Professor Eric Cheney of the University of Washington has been walking the beaches of Puget Sound admiring the local geology for many years. During this time he has discovered that clasts of red rock (RC) are a geologically minor, but very conspicuous component of the beaches of the northern Puget Sound, Washington. As a geologist, Cheney began to record where he has observed RC and began to theorize about their origin. Given the geologic history within the Puget Lowland, RC could have been distributed to their modern location glacially. If the origin of the RC can be established, they may act as a tracer for sediment dispersion into the Puget Lowland from previous glaciations. This report is the culmination of a study into a potential source of RC in the Puget Lowland.

BACKGROUND

Previous Work

Cheney measured the maximum axis of the common RC found on more than 100 beaches around the Puget Sound. He discovered that: (1) the largest clasts (24 cm) are found west of Port Townsend, WA; (2) the RC along the eastern shore of the Olympic Peninsula extend at least as far south as Quilcene, WA; (3) a zone of 12-20 cm RC is centered on the northwestern coast of Whidbey Island; (4) a belt of 12-16 cm RC exists from southern Camino Island to Seattle; (5) in the San Juan Islands, RC are found on San Juan and Lopez island; and (6) on wave-cut beaches south of the Seattle fault, RC are less abundant. He constructed a contour map based on the measured size of red chert clasts across the Puget Sound (Fig. 1).

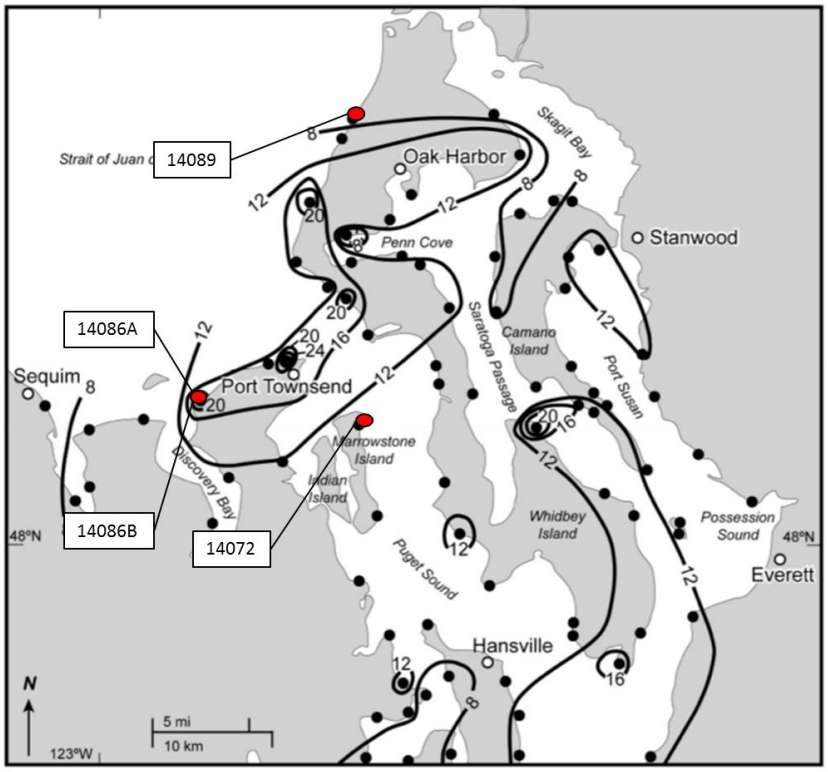

Figure 1 Contour map representing RC of the largest diameter as observed by Cheney. The maximum size of cobbles of red chert on beaches is contoured in 4 cm intervals. Black dots indicate where Cheney has completed 0.5 to 1.5 km long traverses of beaches looking for RC. Red dots indicate location of where the RC used in this study were collected from. Image adapted from Cheney *et al*. (2015).

Due to the glacial history in the Puget Sound area, it is possible that the chert originated from a Canadian source by way of the Puget Lobe of the Cordilleran Ice Sheet, or from alpine glaciers that extended from the western slope of the northern Cascade Mountains. Cheney began to look for red chert described within published literature which led him to the red ribbon cherts of the Fourth Lake Formation on Victoria Island, British Columbia and the red chert described by Vance (1957) in the southwestern portion of the North Cascade Range. Cheney obtained a hand sample from the Fourth Lake Formation (Sample SEG-207) (Figs. 13 and 14) which is described by Massey (1995) as mostly thin-bedded typically cherty sediments that vary from green and red ribbon cherts, black cherty argillites, green and white cherty tuffs, grey and green siltstones and argillites, to thicker bedded green volcanic sandstones. Vance (1957) describes red chert as a component of his Canyon Creek Unit located in the southern portion of the Boulder River Wilderness, off of Mountain Loop Hwy near Verlot, WA (Fig. 2). This study focuses on the comparison between the RC found on northern Puget Sound beaches with a sample from the Fourth Lake Formation and samples from the Canyon Creek Unit of Vance (1957) to determine possible sources. If either the Fourth Lake Formation or the Canyon Creek Unit is a plausible source of RC, a hypothesis about glacier lobe flow paths may be developed which may lead to a better understanding of sediment transport by previous glaciations within the Puget Sound region.

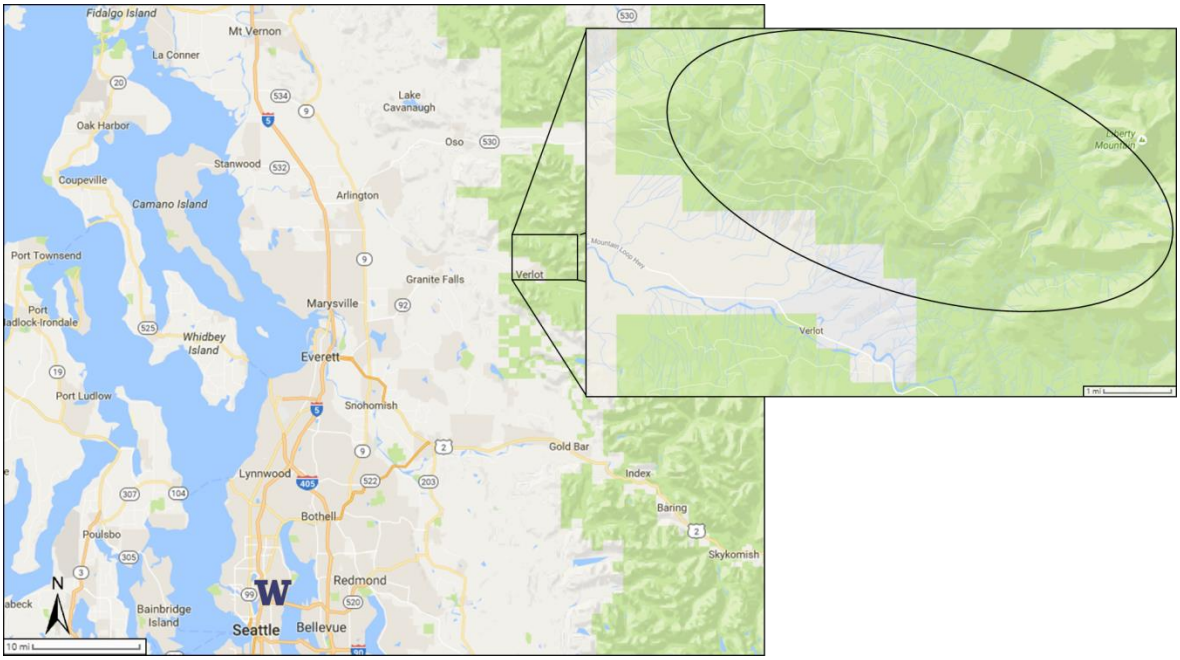

Figure 2 Location of field area relative to the University of Washington. The Canyon Creek Unit of Vance (1957) is by approximately outlined by the oval.

Chert Description

Types of Chert

Chert is the general group name used for siliceous sedimentary rocks and is defined as fine-grained, dense, and commonly very hard rocks composed dominantly of the mineral quartz (SiO_2). Most siliceous rocks may contain minor amounts of impurities such as clay minerals, hematite, calcite, dolomite, and organic matter. Cherts are a common but not abundant rock in the geologic record. Although chert makes up less than 1 percent of all sedimentary rocks, it is represented in stratigraphic sequences ranging from the Precambrian to the present as siliceous oozes in parts of the modern ocean (Boggs, 2009).

According to Boggs (2009) chert is divided based on gross morphology into bedded chert and nodular chert. Bedded chert consists of layers of nearly pure chert up to several centimeters in thickness that are commonly interbedded containing millimeter-thick partings or laminae of siliceous shale. Bedding may be even and uniform or may show pinching and swelling. Many chert beds lack internal sedimentary structures; however, graded bedding, cross-bedding, ripple marks, sole markings, convolute layers, and soft-sediment folds have been reported in some cherts. Because of such structure, mechanical transport may have been involved in the deposition of these rocks. Bedded cherts are commonly associated with ophiolitic rocks such as submarine volcanic flows or pillowed greenstones, tuffs, pelagic limestones, shales, argillites, and siliciclastic or carbonate turbidites. Many bedded cherts are composed dominantly of the remains of siliceous organisms, which are commonly altered to various degrees upon which bedded cherts can be further divided into principal types: (1) diatomaceous deposits that contain preserved fossils of diatoms, a unicellular aquatic plant related to algae, (2) radiolarian deposits, which are marine planktonic protozoans with lattice-like skeletal framework, (3) siliceous spicule deposits (spicularite), a siliceous rock composed principally of the siliceous spicules of invertebrate organisms, particularly sponges, and (4) bedded cherts containing few or no siliceous skeletal remains. Nodular cherts are subspheroidal masses, lenses, or irregular layers or bodies that range in size from a few centimeters to several tens of centimeters. They commonly lack internal structures, but some nodular cherts contain silicified fossils and/or exhibit relict structures such as bedding. They are typically found in shelf-type carbonate rocks where they tend to be concentrated along certain horizons parallel to bedding (Boggs, 2009).

Chert Formation

Radiolarians, diatoms, and silicoflagellates are microplankton that build skeletons of opaline silica. These siliceous microplankton have been abundant enough in the ocean during Phanerozoic time to extract most of the silica delivered to the oceans by rock weathering (Boggs, 2009). Diatoms are probably responsible for the bulk of silica extraction from the modern ocean (Calvert, 1983); however, radiolarians were the most important silica-secreting organisms in the Phanerozoic oceans of Jurassic age and older (Boggs, 2009). Silica solubility is affected particularly by temperature. The solubility of solid SiO_2 at 25ºC in distilled water is ~11 ppm for quartz and ~116 ppm for amorphous or noncrystalline varieties of silica such as opal (Rimstidt, 1997; Gunnarsson and Arórsson, 2000). Solubility increases considerably with increasing temperature: solubility at 100ºC is approximately three times that at 25ºC. Although solubility is also affected by pH, it has minimal changes increasing up to about pH 9, where it drastically increases at pH values greater than 9 (Dove and Rimstidt; 1994, Walther, 2005) Silica is transported by rivers to the modern ocean as silicic acid (H_4SiO_4) in concentrations averaging about 13 ppm SiO_2 (Boggs, 2009). Additionally, silica is added to the oceans through the reaction of seawater with hot volcanic rocks along midocean ridges and by low-temperature alteration of oceanic basalts and detrital silicate particles on the seafloor. Some silica may also escape from silica-enriched pore waters of pelagic sediments on the

seafloor during burial and compaction (Boggs, 2009). Despite the contribution of silica from these various sources, the silica concentration in seawater is quite low. Surface waters are particularly depleted (<0.01 ppm SiO_2) with silica concentration increasing with depth to a maximum of about 11 ppm below 2 km (Boggs, 2009). The variations in silica concentration with depth reflect the uptake of silica near the surface by phytoplankton and regeneration of silica at depth owing to dissolution of the silica skeletons of phytoplankton (Boggs, 2009). The difference between the average silica content of rivers and that of modern seawater reflects the biogenic removal of silica to construct skeletal material of diatoms, radiolarians, and other siliceous organisms (Boggs, 2009).

Once silica is in solution under a given set of temperature and pH conditions, it does not appear to crystallize readily to quartz even from solutions that have silica concentrations exceeding the solubility of quartz (~11 ppm at 25ºC) (Boggs, 2009). Therefore, it is unlikely that chert can be precipitated directly by inorganic processes from highly undersaturated ocean water. Removal of silica from ocean water by silica-secreting organisms to build opaline skeletal structures (opal-A) appears to be the only mechanism capable of large-scale silica extraction from undersaturated seawater. This biologic process has operated since the early Paleozoic and regulates the balance of silica in the ocean.

While silica-secreting organisms are alive, their opaline skeletons are protected from the undersaturated and corrosive seawater by an organic coating. After death, this coating is destroyed by biochemical decomposition and the opaline skeletons begin to undergo dissolution. In areas where siliceous organisms thrive, the production rates of siliceous skeletons may be so high that they are not dissolved as rapidly as they are produced. Under such conditions, sufficient amounts of opaline skeletal material may accumulate on the seafloor as siliceous oozes. After burial by additional siliceous ooze or clayey sediment, the opaline skeletal material continues to undergo dissolution; however, the dissolving silica is trapped in the pore spaces of the sediment and cannot all escape back to the open ocean (Boggs, 2009). The pore waters thus become enriched in silica, with values as high as 120 ppm reported in pore fluids extracted from recovered deep-sea cores (Gieskes, 1983). Such pore waters are saturated to supersaturated with respect to silica, and cherts are thought to precipitate slowly from these concentrated interstitial solutions. Thus, the formation of cherts is in part a sedimentation process involving the depositional concentration of biogenic opaline skeletons and in part a digenetic process of recrystallization of the chert after sediment burial (Boggs, 2009). The process of crystallization and recrystallization of opaline skeletal material to chert is illustrated in Figure 3.

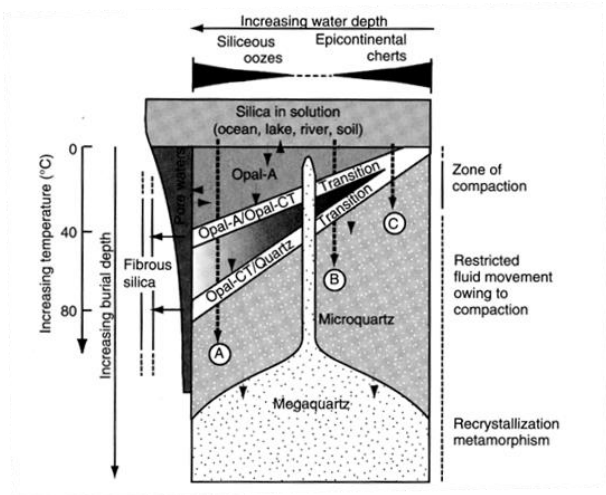

Figure 3 Schematic diagram showing major silica phases and their possible diagenetic transformations. Vertical dimension represents qualitative burial depth with associated increase in temperature and loss of porosity and permeability. Horizontal dimension represents qualitative water depth of the initial environment. Adapted from Boggs (2009).

GEOLOGIC HISTORY

The geology of Washington state can be described in four phases: (1) the pre-Jurassic rocks indigenous to ancestral North America (Laurentia), (2) terranes that accreted to Laurentia in the past 185 Ma by plate tectonic processes, (3) sedimentary and volcanic rocks less than 56 Ma, which discontinuously cover Laurentia and the accreted terrains, and (4) sedimentary and volcanic rocks deposited within the past few million years. Also present are numerous granitic rocks formed 185 to 2 Ma that intruded along the continental margin (Cheney, 2016).

Mesozoic Geology

This study focuses on the rocks southwest of the Darrington-Devils Mountain Fault Zone (DDMFZ) in the Western Domain (Fig. 4). The accretion of terranes to the Pacific Northwest portion of the North American plate began in the mid-Jurassic (174.2 Ma) (Cheney, 2016). Pieces of exotic plates, or terranes that make up the Cascade Range were accreted subsequently. These terranes are made up of accreted volcanic island arcs, deep ocean sediments, basaltic ocean floor, and parts of protocontinents, submarine fans, and even pieces of the deep subcrustal mantle of the Earth (Tabor and Haugerud, 1999). Three domains, or packages of terranes brought together along a number of faults make up the Cascade Range: (from east to west) the Methow, Metamorphic Core, and Western Domains.

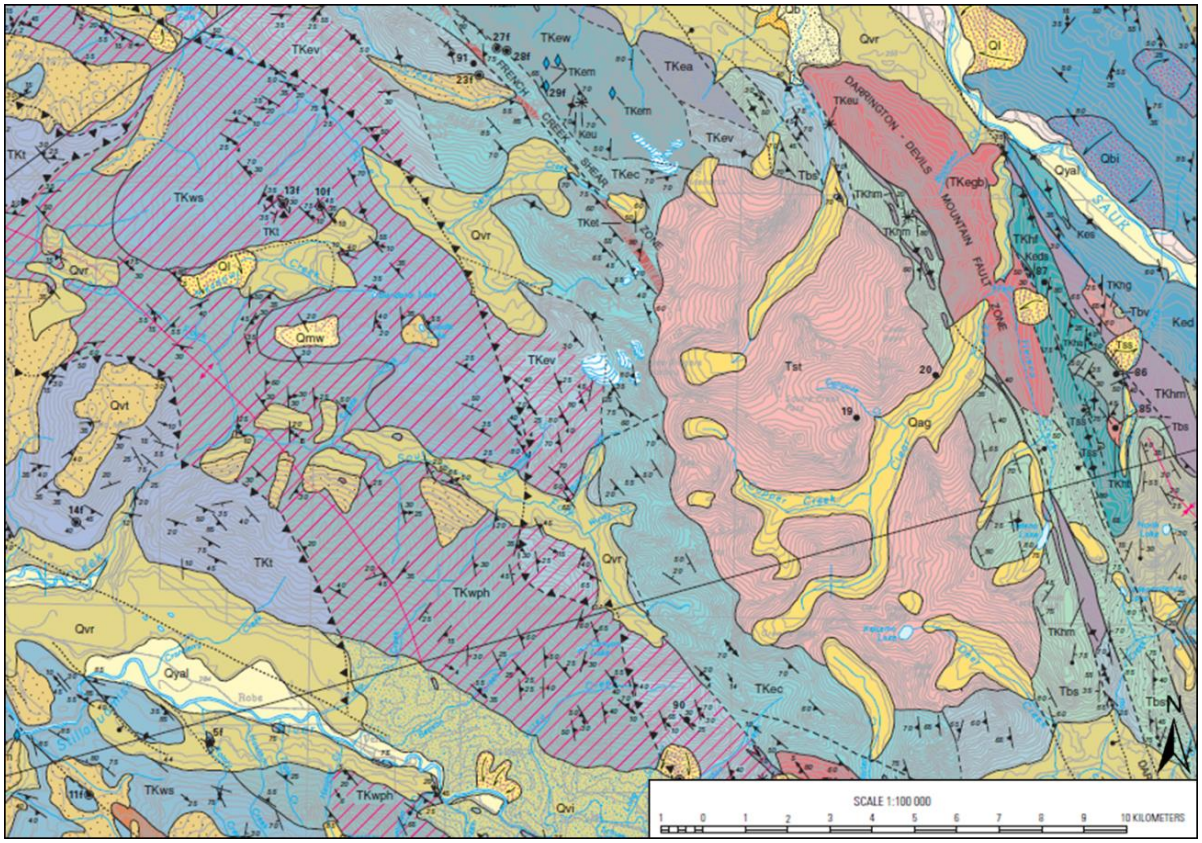

Figure 4 Geologic map adapted from Tabor *et al.* (2006) showing rocks southwest of the Darrington Devils Mountain Fault Zone. Refer to Fig. 48 in the appendix for map legend.

Southwest of the DDMFZ, the western and eastern mélange belts (WEMB) are composed of oceanic rocks characterized by extreme disruption on an outcrop scale and low P-T metamorphic assemblages (Tabor *et al.,* 2006). The Western mélange belt is mainly Late Jurassic to Early Cretaceous marine sedimentary components and common thick-bedded volcanic subquartzose sandstone; mafic volcanic rocks and chert are locally abundant but overall are minor constituents. A regional antiform exposes a pelitic facies, characterized by a pervasive phyllitic cleavage (Tabor, 1994). The Eastern mélange belt (including the Trafton terrane of Whetten *et al.*, 1988) is characterized by abundant mafic volcanic rocks, chert, and scattered ultramafic by rocks ranging from Mississippian to Early Jurassic (Tabor and Haugerud, 2016), and is locally less penetratively deformed (Tabor *et al., 2006).* The Eastern mélange belt and the highly mixed Trafton terrane, appear to be structurally high and folded over the regional antiform expressed in the Western mélange belt. Tabor *et al.,* (2006) consider the Eastern mélange belt and Trafton terrane to be in fault contact with the underlying Western mélange belt, although the disruption between the two units along this inferred fault is no more severe than that within the mélanges themselves. With the development of phyllitic foliation and metamorphic pumpellyite and prehnite in parts of the WEMB, regional metamorphism probably contributed to the disruption and mixing of the rocks (Tabor, 1994). In both mélange belts, blocks of harder rocks are set in a matrix of scaly argillite or phyllite and generally range from a few centimeters across to many kilometers across (Tabor, 1994).
In the Western mélange belt, rare fossil ages from argillite and several from chert are mostly Late Jurassic and Early Cretaceous. Meta-igneous blocks in the Eastern mélange belt are Late Triassic whereas fossils in argillite, chert, and rarely in limestone of the eastern mélange belt range in age from Mississippian to Late Jurassic, and fossils in the Trafton terrane are dated from Mississippian to Early Jurassic (Tabor, 1994). The age of mélange formation for the Eastern and Western belts and the Trafton mélange can only be restricted to a time span between the youngest component of the mélange and the oldest overlying unit. Tabor *et al.* (2006) assume that all the mélanges south of the DDMFZ formed at about the same time, which is between mid-Cretaceous and Eocene.

Cenozoic Geology

During the early Oligocene establishment of the Cascade arc, a series of intrusive events created numerous plutons in the western Cascades (Vance *et al.,* 1986). One such pluton, the Squire Creek tonalite (unit Tst) (Fig. 4) is present in the eastern extent of the field area and is related to magmas of the Mount Index batholith (Tabor *et al.,* 1989). Other igneous and metamorphic blocks are diabase, metatonalite, and amphibolite, tonalitic gneiss, and associated leucotonalite dikes. Few exposures reveal contacts, but all blocks are cut by many brittle shears, commonly with chloritic alteration (Tabor, 1994).

Quaternary Geology

Upper Pleistocene strata from the four glacial and five non-glacial sequences are found within the Puget Sound. The last and most germane to this study is the Fraser Glaciation, which consists of four stades: (1) the Evans Creek Stade, an early alpine advance in the Cascades, (2) the Vashon Stade, the maximum advance of the Cordilleran ice sheet, (3) the Everson Interstade, an interval of glaciomarine deposition in the Puget Lowland, and (4) the Sumas Stade, during which several brief readvances of the CIS in the Fraser Lowland occurred (Table 2) (McCormack and Troost, 2016). Although the Holocene began about 11.7 ka, in the Puget Lowland, the Puget lobe of the Cordilleran ice sheet had retreated out of the current Puget Sound by about 13 ka (Porter and Swanson, 1998), and sedimentation changed from glacial to non-glacial. Within the Puget Lowland stratigraphy, this glacial to non-glacial transition is generally a proxy for the Pleistocene—Holocene boundary (McCormack and Troost, 2016).

METHODS

Geologic and topographic maps of the area were obtained to determine where any red chert has been described and how to access any areas of interest. Areas of interest were identified based the mention of siliceous red rocks in Vance (1957) and in the Sauk River 30-minute by 60-minute quadrangle, Washington produced by Tabor *et al.* (2006). The Canyon Creek Unit is a thick series of sedimentary rocks comprising of slates and argillites, ribbon cherts, and dark feldspathic sandstones. Red chert is not uncommon in the western margins of the unit furthest away from a tonalite intrusion (Unit Tst) (Fig. 5). Vance (1957) argues that it is possible that the red coloration of the chert has been lost near unit Tst by incipient recrystallization caused by contact metamorphism. Tabor *et al.* (2006) divided the Canyon Creek Unit of Vance (1957) into separate units (TKev, TKec, and TKwph respectively) (Fig. 4). For these reasons I have focused my search in the western half of the Canyon Creek Unit. (Refer to Table 3 in the Appendix for all locations visited, and short descriptions). I was given RC from various Puget Sound beaches collected by Cheney as a reference for what I was to look for and to become familiar with rock preparation and thin section manufacture.

Field methods

I began by identifying fluvial systems whose watersheds overlapped with the Canyon Creek Unit. I searched the rivers and streams for red rocks that are similar to the RC samples attained from Cheney. I followed the fluvial systems upstream to locate any bedrock exposures, outcrops, boulders of red rock, and/or limit of RC presence. When I determined the extent of RC within the searched fluvial systems, I began searching all the forest roads and trails that could be located within the area of interest. Areas or points of interest were accessed by dirt bike due to many road washouts and overgrown trails. More remote locations had to be accessed on foot during multi-day backpacking trips. Due to the remote location of some of the points and transportation method used, only essential geologic equipment could be packed due to weight concerns. Therefore, essential geologic equipment with the aid of a handheld Garman GPS device was used to obtain and record data.

Observation methods

When RC samples were found, I measured the long axis of the largest clasts, photographed them, and recorded a short description. I recorded a detailed description of the overall site as well as GPS coordinates and photographs. I followed rivers and streams containing RC upstream as far as possible to locate any outcrops containing rocks of interest. Outcrops containing *in situ* red rocks were identified via GPS, measured horizontally and vertically (when possible), photographed, and described. Any samples collected were marked with a station number and packed out to be further described at a smaller scale and prepped for thin section manufacture.

Analysis methods

The color of the beach cobbles and collected samples was determined using a Munsell color chart, then the sample was cut, photographed, and prepped for thin section manufacture. Because the samples are composed of very hard, densely packed fine-grained siliceous material, thin section manufacture proved to be labor intensive with a high failure rate. I decided to have the thin sections manufactured professionally by National Petrographic, Inc. in Houston, TX. The completed thin sections were compared against each other using a petrographic microscope and the expertise of Dr. Charlotte Schreiber to determine similarities and differences.

RESULTS

Identified areas and points of interest fall into one of two main categories: river bed/gravel bar or outcrop/road cut (Fig. 5). I searched gravel bars within the NFSR and SFSR for RC to establish which drainages might contain *in situ* red chert. Additionally, I also searched the Skykomish and Sauk Rivers for RC to determine if the red chert exists outside of the Boulder River Wilderness. RC are found within the bed load of North and South Fork of the Stillaguamish River and were not in either the Sauk or Skykomish Rivers. The North Fork Stillaguamish yielded RC sparingly; the largest clast measured 9cm was at location B-5-16. RC abundance drastically reduced upstream and was not found at all near Whitehorse, WA. A section of very large boulders (Figs. 28 and 31) of red chert measuring up to 4m are present in the South Fork Stillaguamish River (B-37-15). Boulders of this large size are only located in a relatively small reach of the river, extending upstream approximately 50m where the overall size of boulders reduced drastically to cobbles <10cm. Downstream the boulder density extends approximately 100m before reducing in size to cobble-sized clasts. *In situ* red rocks (chert, argillite or phyllite) are found in various regions throughout the Canyon Creek Unit (Fig. 4) both along in-use and abandoned forestry roads. Although the majority of exposed red bedrock found is located north and west of the boulder field found in the N. Fork Stillaguamish River within the TKwph unit, red bedrock exists within the TKt and TKev units as well.

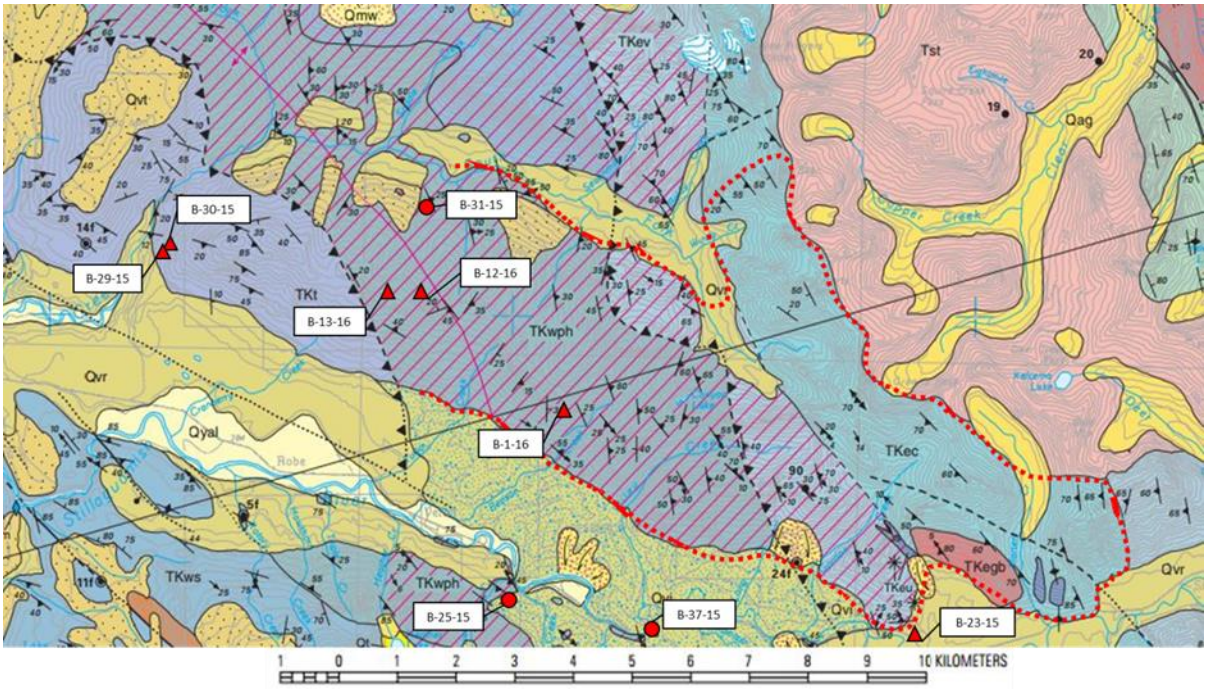

Figure 5 Geologic map adapted from Tabor *et al*. (2006) showing sample locations. Triangles indicate bedrock sample locations, circles indicate cobble or boulder sample locations, and the dotted red line outlines the mapped extent of the Canyon Creek Unit. Refer to Fig. 48 in the appendix for map legend

Sample descriptions

Samples collected by E. Cheney

Figure 6 14072 hand sample photo, 2.5YR 3/6 (dark red).

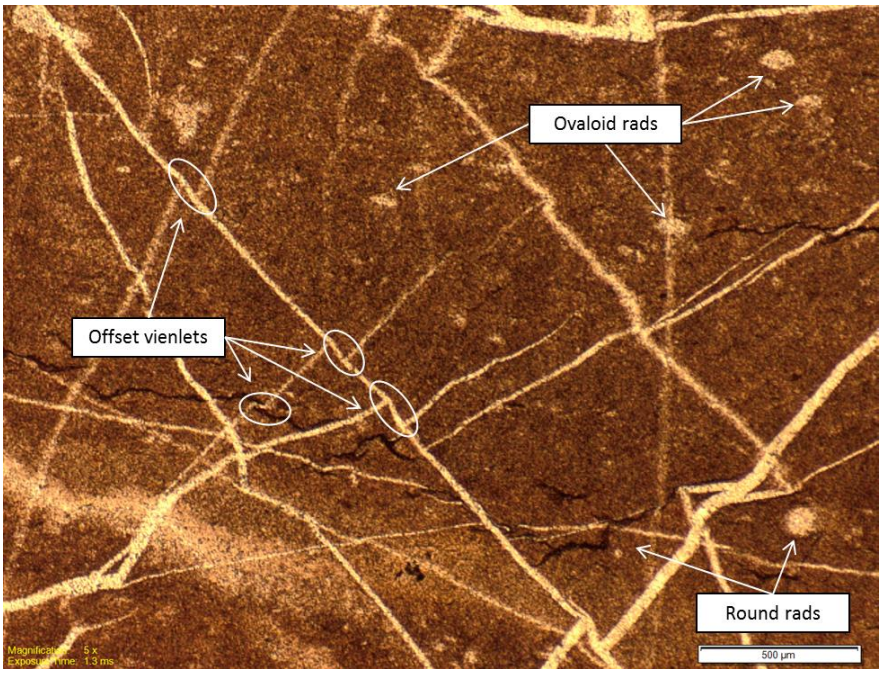

Figure 7 Sample 14072 thin section image showing round and ovaloid radiolarian remnants and offset veinlets.

14072 (Figs. 6 and 7) – Collected from Fort Flagger State Park, Marrowstone Island, WA – Foliated, fine grained, grading in color from maroon to pale pink to dark grey in thin section, very few round to ellipsoidal radiolarian remnants that are extended along the same plane within the matrix. 50% of the section is inundated with veinlets of white quartz that range in thickness from <<1mm to 3mm containing various sizes of quartz crystals. Most of the quartz veinlets are offset along very thin black fractures. Thin section contains a highly deformed zone bounded by dark fractures that is composed primarily of synformal quartz veinlets surrounding jagged pieces of pink to grey ground mass.

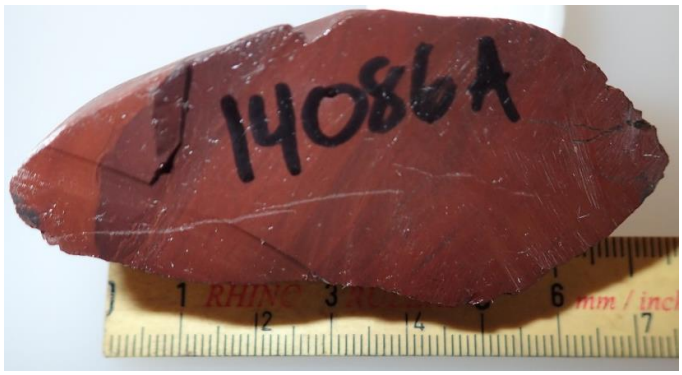

Figure 8 14086A hand sample photo, 2.5YR 2.5/3 (dark reddish brown). Lighter and darker bands are the result of the difference in clastic material abundance as observed in figure 9.

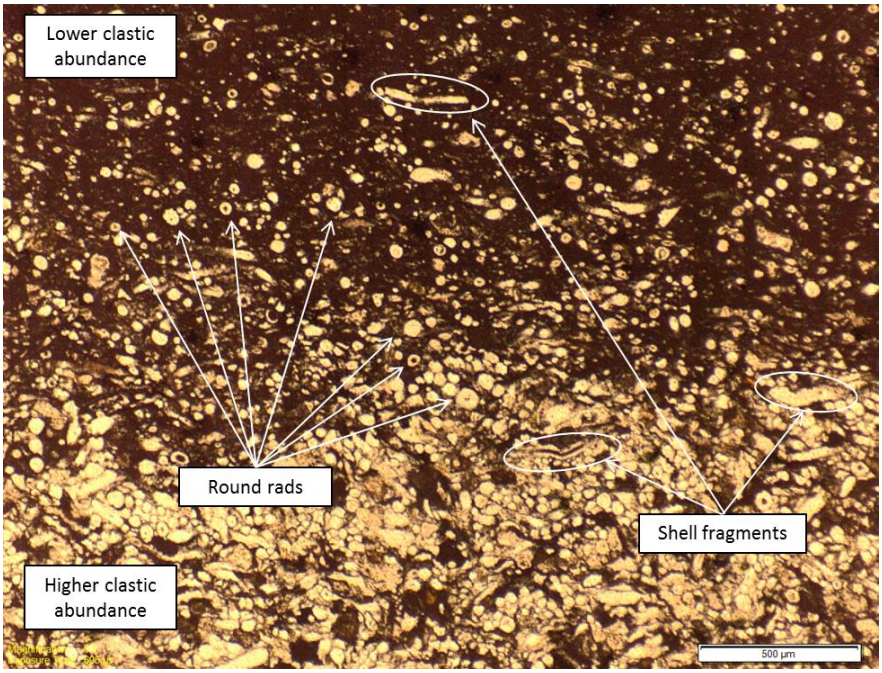

Figure 9 Sample 14086A thin section image showing round radiolaria and shell fragments graded with clastic material.

14086A (Figs. 8 and 9) – Collected from Cape George, Olympic Peninsula, WA - Slightly foliated, fine grained, grading in color from maroon to bright red and pale bands. The pale bands are mainly composed of spherical relics of radiolaria and minor ellipsoidal radiolarian remnants, a few other broken but replaced shell fragments, and larger subrounded clastic quartz grains. Darker bands are composed of minor fragmentary radiolarian remnants (7%) in a fine grained foliated matrix of a dark brown, very fine-grained mineral. Separated into layers marked by a black-colored cement that is parallel with the major foliation plane. No quartz veinlets are present.

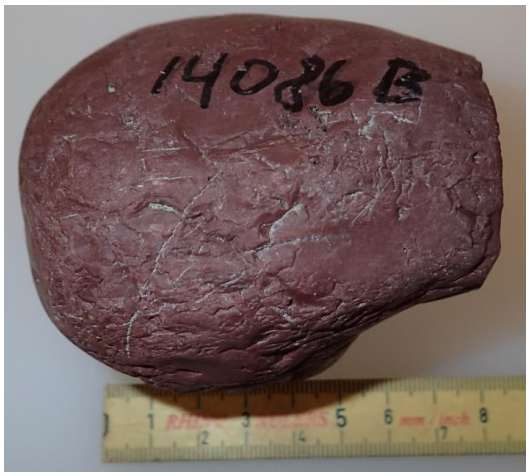

Figure 10 14086B hand sample photo, 10R 3/3 (dusky red).

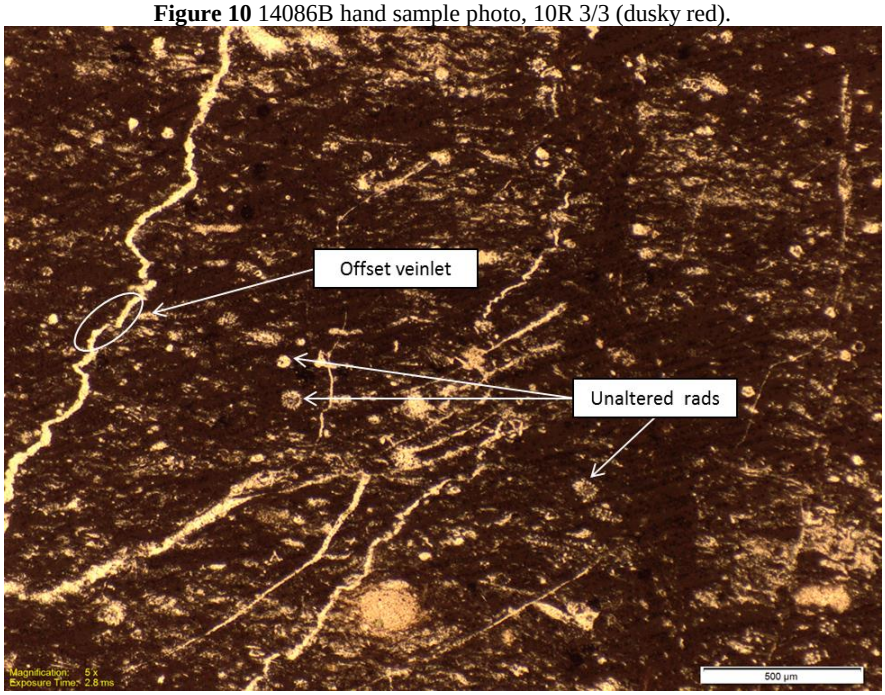

Figure 11 Sample 14086B thin section image showing unaltered radiolaria skeletons, and offset veinlets.

14086B (Figs. 10 and 11) – Collected from Cape George, Olympic Peninsula, WA - Foliated, fine grained, a dark maroon matrix which has a slightly linear fabric that is modified by pale swirls. Matrix is composed of 20% radiolarian remnants of various sizes that are stretched in concert with the orientation of the fabric and lighter swirls, and 80% dark opaque maroon mineral. Thin section contains many very fine white quartz veinlets that do not have a specific overall orientation and connect to relatively larger quartz nodes made up of large quartz crystals. Some veinlets are offset along tight planes that have not been filled in with another mineral.

Figure 12 14089 hand sample photo, 2.5YR 2.5/4 (dark reddish brown).

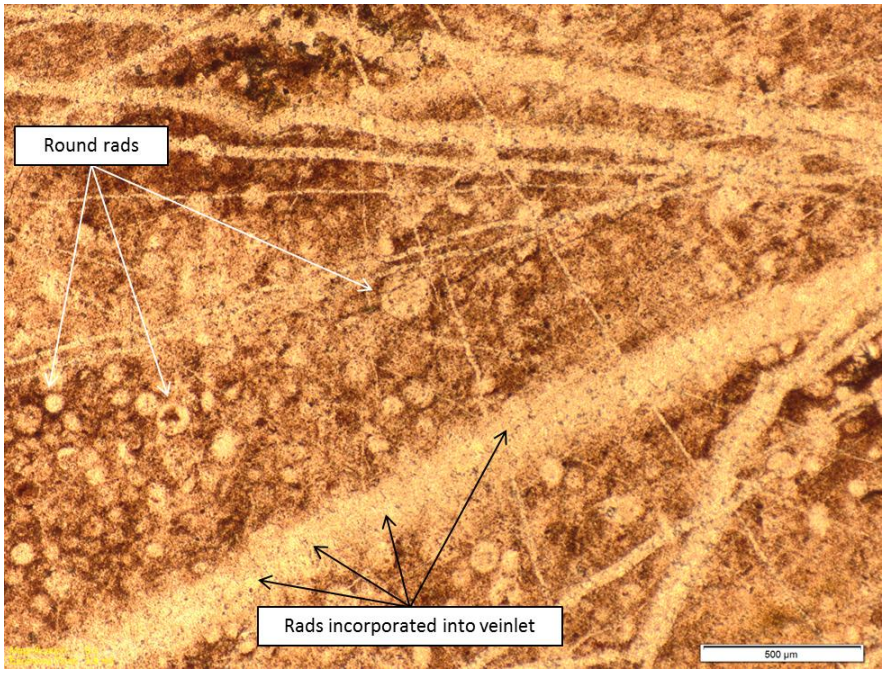

Figure 13 Sample 14089 thin section image showing round radiolaria, and radiolaria that are incorporated into veinlets.

14089 (Figs. 12 and 13)– Whidbey Naval Air Station, Whidbey Island, WA - Fine grained pale red matrix containing abundant spherical radiolaria that is cut by white quartz veinlets of random orientations. No foliation or bedding is observable. Because of the roundness of the radiolarian it can be said that the veinlets probably formed prior to compaction.

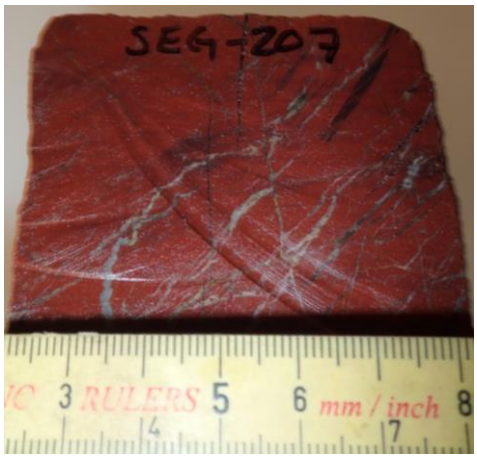

Figure 14 SEG-207 hand sample photo, 10R 3/4 (dusky red).

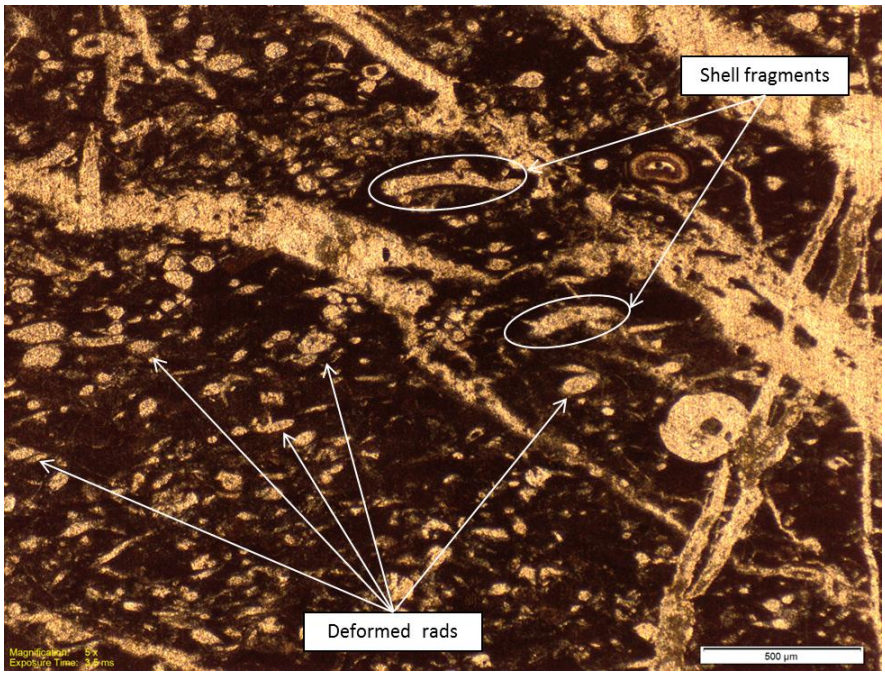

Figure 15 Sample SEG-207 thin section image showing deformed radiolaria and shell fragments.

SEG-207 (Figs. 14 and 15) – Fourth Lake Formation, Victoria Island, British Columbia, Canada – Foliated, fine grained, graded from bright red to dark grey matrix containing a linear foliation containing abundant radiolarians that are orientated along the plane of foliation. The section contains three main orientations of white quartz veinlets, (1) abundant parallel veinlets angled ~35º off the fabric orientation, (2) a secondary set of parallel veinlets these intersect the majority at ~90º, and (3) a minor set of veinlets that intersect the foliation plane at ~90º. Section also contains an additional porphyroblasts that are larger, spherical, and composed of microcrystalline quartz with a central opaque mineral around which an additional microcrystalline quartz rind is observable.

Samples collected by writer

Figure 16 Sample B-23-15, Field photo of red bedrock exposure. Red dashed line outline red band in outcrop. E. Cheney for scale.

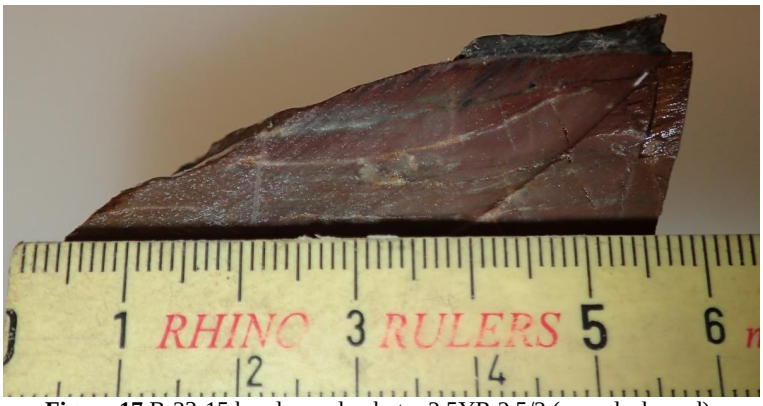

Figure 17 B-23-15 hand sample photo, 2.5YR 2.5/2 (very dusky red).

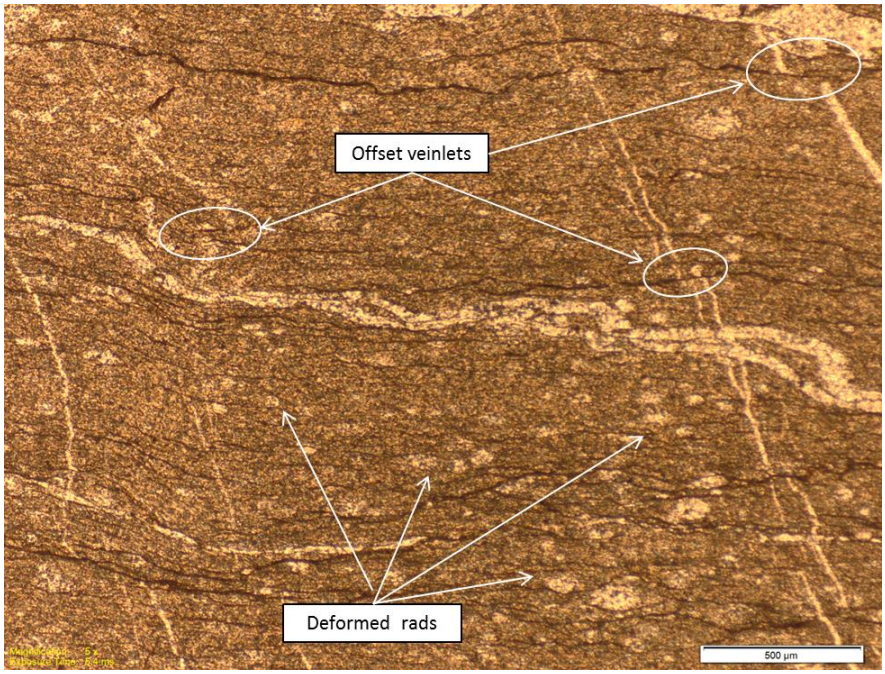

Figure 18 Sample B-23-15 thin section image showing deformed radiolaria in a foliated fabric and offset quartz veinlets.

B-23-15 (Figs. 16-18) – Sampled from a red bedrock exposure unit TKev of Tabor *et al.* (2006). Foliated, fine grained, graded from pale pink to pale red fabric composed of ~10% composition of stretched oval radiolaria in a linear (with small variations) plane of foliation. Section contains a moderate amount of white quartz veinlets parallel the foliation plane. Fewer long fine thin white quartz veinlets that are offset in the direction of foliation. These veinlets are cross-cut by thicker rope-like sinuous white quartz veinlets, some of which have been intruded along the plane of foliation.

Figure 19 Sample B-25-15, field photo of large red boulder on Lake 22 trail.

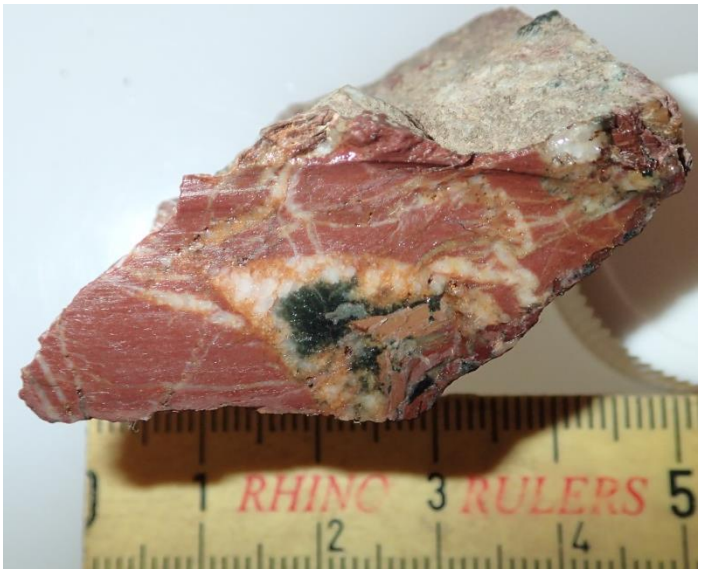

Figure 20 B-25-15 hand sample photo, 10R 3/4 (dusky red).

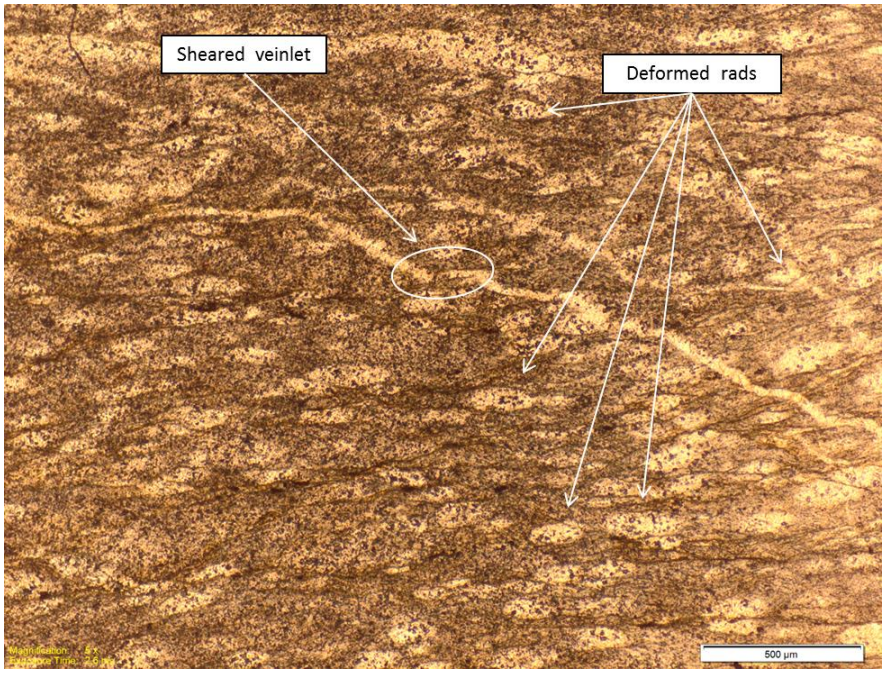

Figure 21 Sample B-25-15 thin section image showing deformed radiolaria and sheared veinlet.

B-25-15 (Figs. 19-21) – Red boulder on Lake 22 trail mapped within the TKwph unit of Tabor *et al.* (2006). Foliated, fine grained, uniformly pale red fabric composed of ~30% composition of deformed oval radiolaria in a sinuous foliation plane. The section contains a moderate amount of fine white quartz veinlets that run perpendicular to the foliation plane and are further offset in the direction of foliation. The majority of the veinlets are relatively thick, sinuous, and may contain large quartz crystals. The quartz crystal size is relative and proportional to the size of the veinlet it which it resides.

Figure 22 Sample B-29-15 and B-30-15, Field photo of red bedrock exposure in roadbed rock hammer for scale.

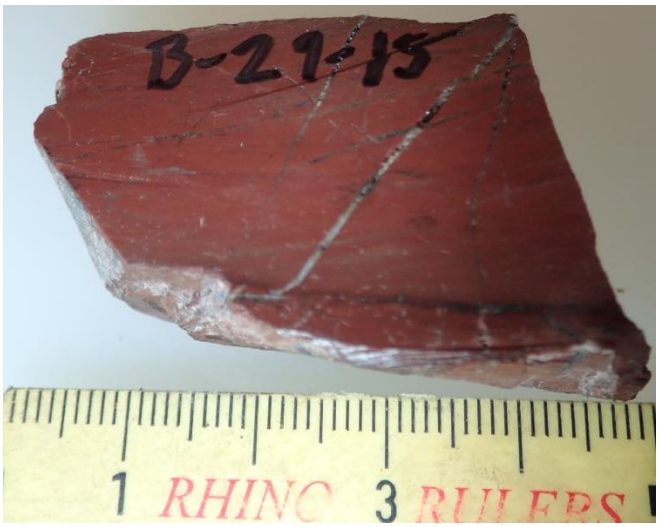

Figure 23 B-29-15 hand sample photo, 2.5YR 3/4 (dark reddish brown).

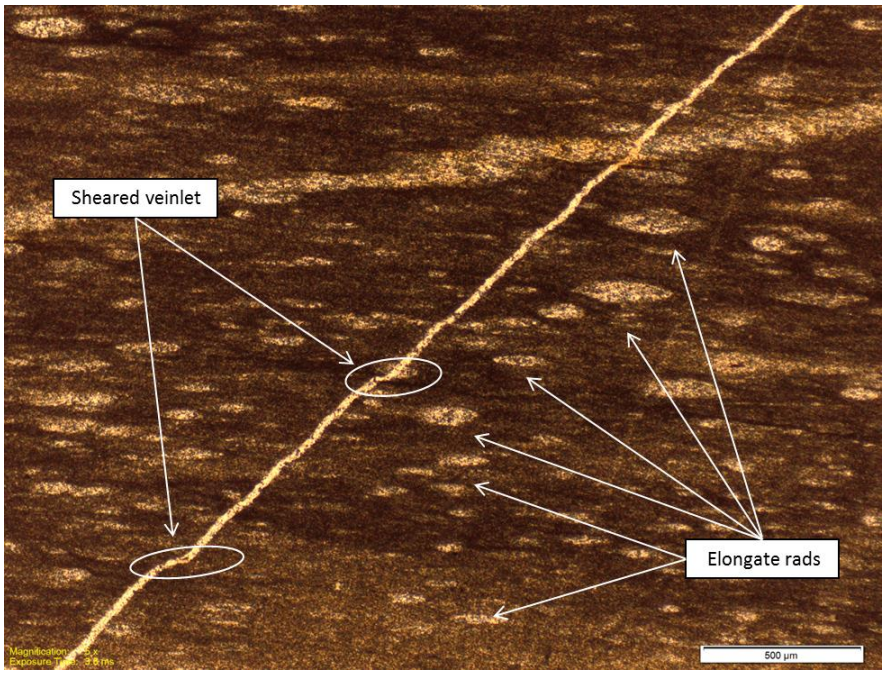

Figure 24 Sample B-29-15 thin section image showing a sheared veinlet and elongate radiolaria.

B-29-15 (Figs. 22-24) – Red bedrock exposure in road bed mapped within TKt unit. Foliated, fine grained, graded in color along foliation from red to pale pink. The darker regions are composed ~5% composition of extremely stretched radiolaria, and the lighter regions are composed ~40% extremely stretched radiolaria. Faint, moderately thick white veinlets that are pervasively affected by the foliation, and incorporate radiolaria where they are in higher concentrations. Thinner white quartz veinlets intersect the foliation plane containing no alteration or offset by foliation, but they are cross-cut and offset by very thick quartz veinlets containing darker unknown minerals.

Figure 25 B-30-15 hand sample photo, lighter color - 10R 3/3 (reddish brown), darker color – 10R 3/1 (dark reddish gray).

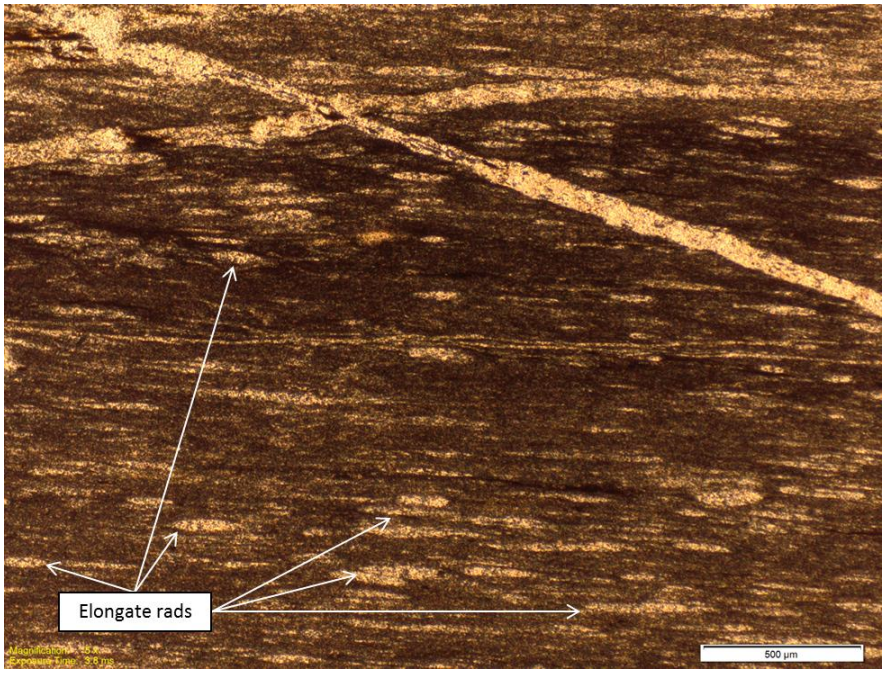

Figure 26 Sample B-30-15 thin section image showing elongate radiolaria.

B-30-15 (Figs. 25-26) – Red bedrock exposure in road bed mapped within TKt unit. Foliated, fine grained, uniformly pale maroon sinuous fabric comprising of ~30% extremely stretched fossils (radiolaria). The fabric is pervasively penetrated by few thin, linear white quartz veinlets, and an abundance of thick sinuous quartz veins. The entire section is cross cut by thick bands of dark opaque iron- or manganese-rich veinlets that are sheared. At least two generations of deformation are present within the thin section.

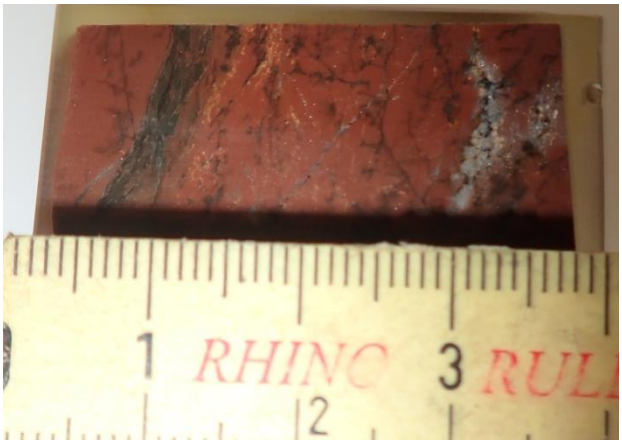

Figure 27 B-31-15 hand sample photo, 2.5YR 3/6 (dark red)

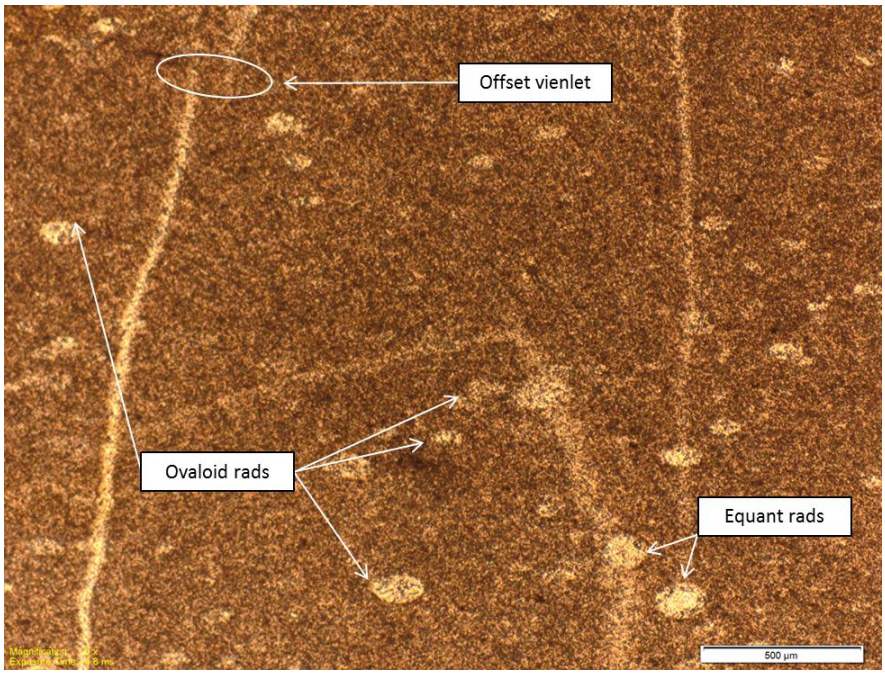

Figure 28 Sample B-31-15 thin section image showing equant and ovaloid radiolaria, and offset veinlets.

B-31-15 (Figs. 27 and 28) – Cobble found in stream bed mapped within the TKwph unit of Tabor *et al.* (2006), lightly foliated, fine grained, uniformly pale red matrix comprising of ~10-15% spherical and slightly stretched oval radiolaria, some of which have been replaced by an unknown dark opaque mineral. The long axes of oval radiolaria align in the same general direction, but there is a lack of directional fabric observed. Faint veinlets filled with microcrystalline quartz are cross-cut by more defined quartz veinlets, some of which are offset in the direction of stretched radiolaria. The section contains a zone of microcrystalline quartz composed of both spherical and ovoid radiolaria in a greenish of microcrystalline quartz intertwined a dark mineral.

Figure 29 Sample B-37-15A, field photo of an extremely large red boulder in the South Fork Stillaguamish River measuring 3.55m x 2.63m x 1.42m. Writer for scale. (photo courtesy of Jim Miller).

Figure 30 B-37-15A hand sample photo, lighter color – 10R 3/3 (reddish brown), darker color - 2.5YR 3/6 (dark red).

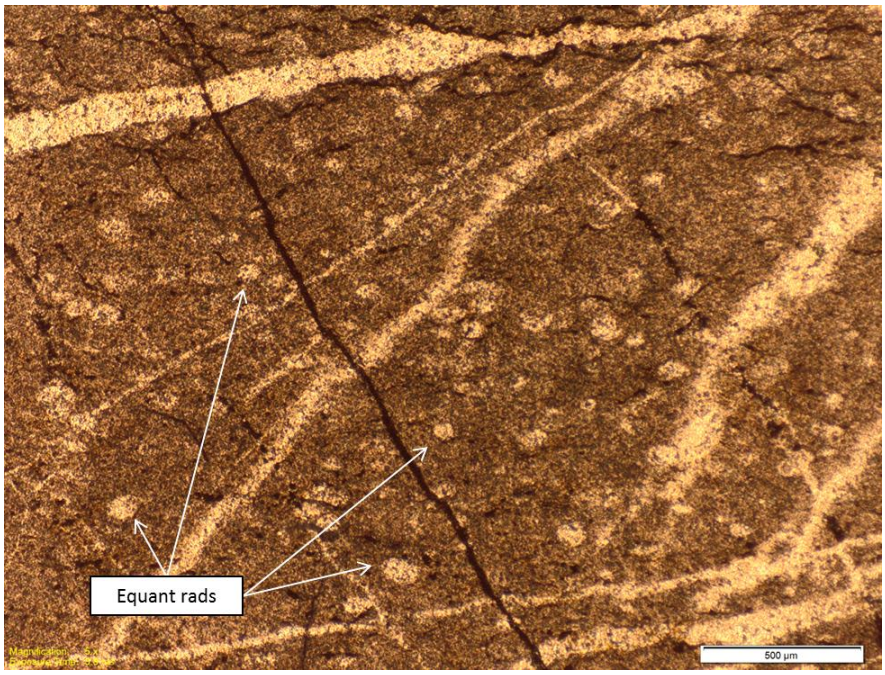

Figure 31 Sample B-37-15A thin section image showing equant radiolaria.

B-37-15A (Figs. 29-31) – This sample is from an extremely large red boulder in the bed of the North Fork Stillaguamish River (Fig. 29-31). Foliated, fine grained consisting of three major zones. (1) Darker yellow-green zones composed of >50% mostly spherical and minor slightly oval radiolaria that are separated and distinct from the rest of the section, quartz veinlets do intersect this zone, but they are more altered than the extent of the veinlets in other zones. (2) Pale red matrix composed of ~25% radiolaria that are more stretched that those found in zone 1, although some spherical radiolaria do exist. This zone is pervasively and randomly cross-cut by varying thickness mostly linear quartz veinlets. (3) Mostly white microcrystalline quartz, and subordinate very light pale pink pieces of zone 2 that are more altered.

Figure 32 Sample B-37-15B, field photo of a large red boulder along the bank of the South Fork Stillaguamish River, Boulder measures 1.67m x 1.42m x 1.00m.

Figure 33 B-37-15B hand sample photo, 2.5YR 2.5/4 (dark reddish brown).

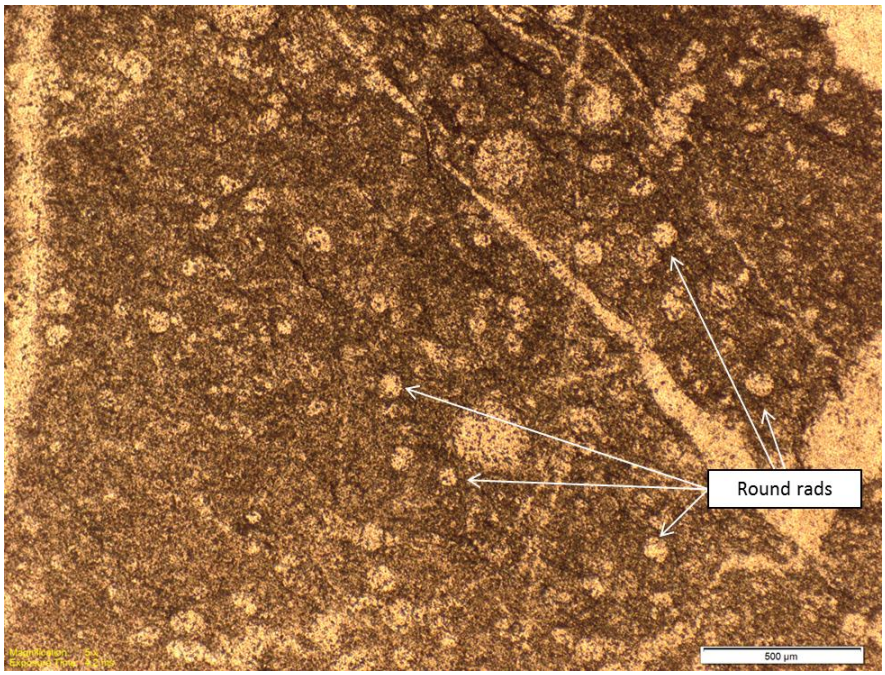

Figure 34 Sample B-37-15B thin section image showing round distorted radiolaria

B-37-15B (Figs. 32-34) – Large Boulder found in river-bed, Fine grained, pale red, matrix composed of ~20% spherical very slightly deformed radiolaria. The radiolaria do not show any direction of strain and slightly vary in size. The matrix is randomly intersected by white quartz veins that vary in size from very thin to very thick. The quartz crystals within the veinlets are relative and proportional to the thickness of the veinlet in which it resides.

Figure 35 Source of sample B-1-16A and B-1-16B field photo of outcrop. Red dashed line indicates band of banded red rock shown in figure 35), scree slopes in bottom of photo are mostly composed of red rocks from above.

Figure 36 Source of samples B-1-16A and B-1-16B, field photo of a band of bedded red bedrock exposure, ruler indicates cm scale.

Figure 37 B-1-16A hand sample photo, lighter color – 2.5YR 3/6 (dark red), darker color - 2.5YR 2.5/3 (dark reddish brown)

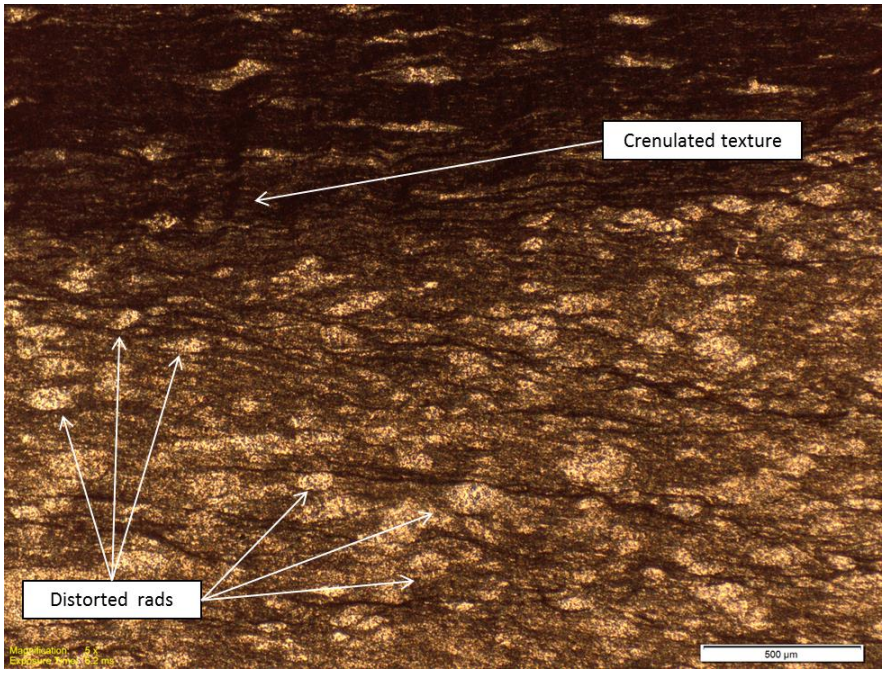

Figure 38 Sample B-1-16A thin section image showing crenulated texture and distorted radiolaria.

B-1-16A (Figs. 35-38) – Band of bedded red bedrock exposure mapped within TKwph unit of Tabor *et al*. (2006), highly foliated, fine grained, banded dark red to pink with dark bands of higher foliation. Fabric contains ~30% extremely stretched radiolaria in the lighter bands and <15% stretched radiolaria that are almost unrecognizable because of the distortion. The darkest band does not exhibit any recognizable radiolaria as it has a higher degree of foliation. The section contains few very thin linear white veinlets, filled with extremely microcrystalline quartz that follow the foliation plane.

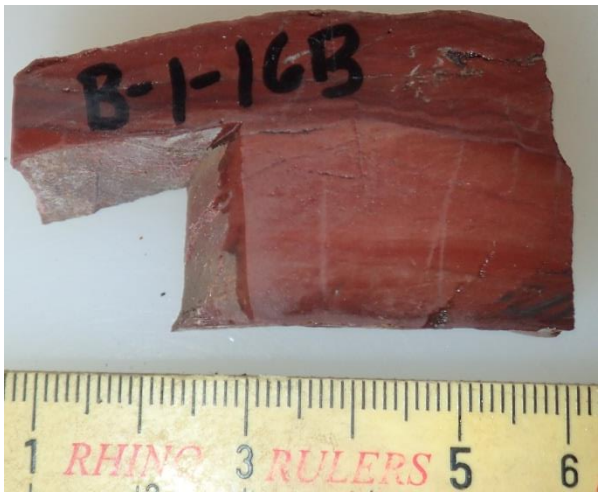

Figure 39 B-1-16B hand sample photo, lighter color – 2.5YR 4/3 (reddish brown), darker color – 2.5YR 2.5/3 (dark reddish brown).

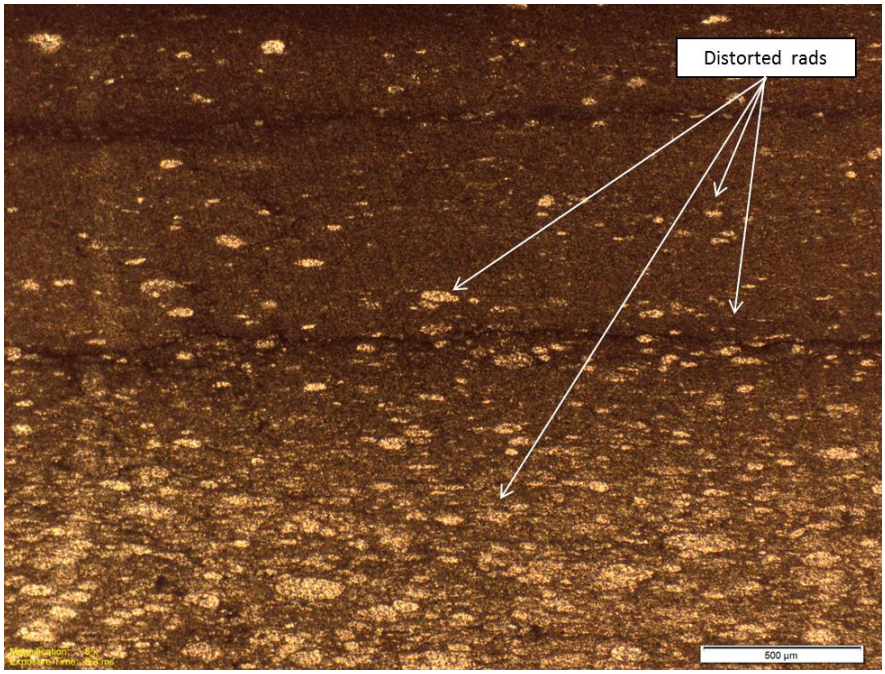

Figure 40 Sample B-1-16B thin section image graded distorted radiolaria.

B-1-16B (Figs. 35, 36, 39-40) – Band of bedded red bedrock exposure mapped within the TKwph unit of Tabor *et al.* (2006). Foliated, fine grained, banded dark maroon to pale pink. The section contains varying numbers of radiolaria that show different degrees of deformation. The radiolaria population is not restricted to any particular band or color and appears to grade up and down perpendicular to the plane of foliation, which changes from mostly linear to sinuous. The section also contains crenulation cleavage within the darkest regions of the section.

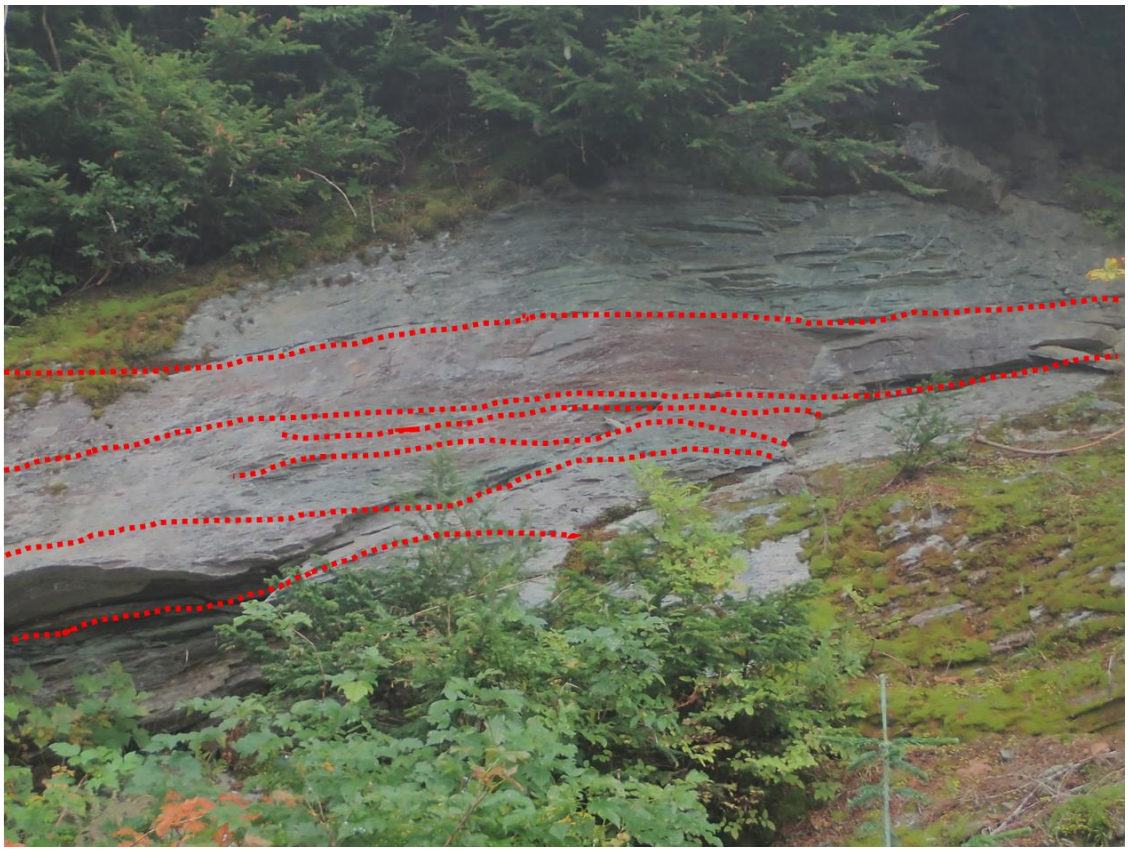

Figure 41 Source of sample B-12-13, field photo of outcrop, red dashed lines highlight bands of red rock shown in figure 42.

Figure 42 Source of sample B-12-16, close up field photo of red bedrock exposure (Fig. 41). Ruler indicates cm scale.

Figure 43 B-12-16 hand sample photo, 10R 3/4 (dusky red).

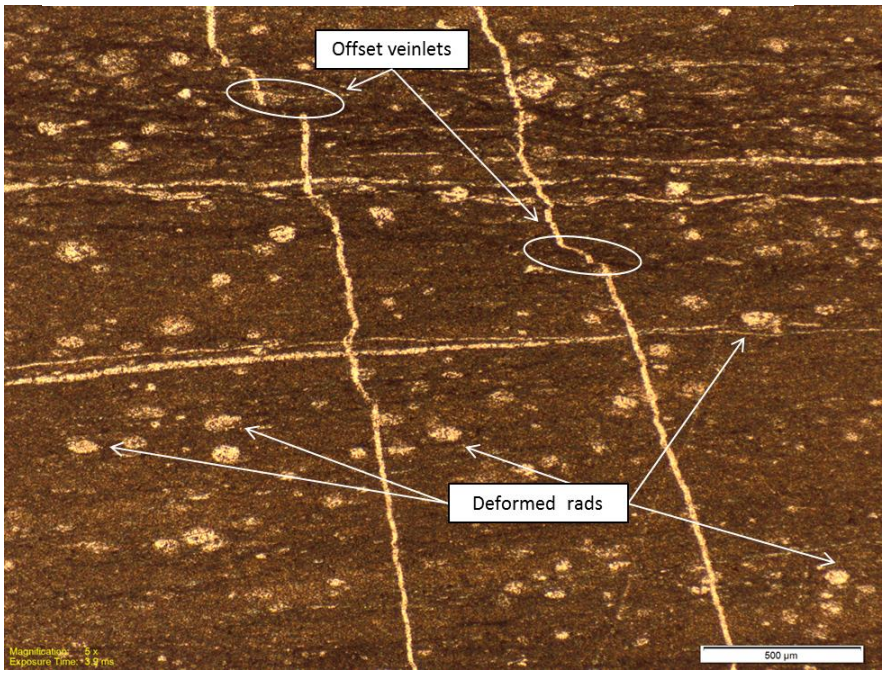

Figure 44 Sample B-12-16 thin section image showing deformed radiolaria and offset veinlets.

B-12-16 (Figs. 41-44) – Bedrock exposure mapped within the TKwph unit of Tabor *et al.* (2006). Foliated, fine grained, banded perpendicular to foliation, pale purple to pale pink, and some dark green layers. Overall fabric is composed of ~10-20% aligned ovaloid radiolaria, the dark green bands containing the higher percentages. Foliation plane is mostly linear that grades to slightly sinuous. Thin quartz veinlets run perpendicular to the direction of foliation, and thicker veinlets are parallel to foliation.

Figure 45 Source of sample B-13-16A field photo of a bedrock exposure in road bed.

Figure 46 B-13-16A, hand sample photo, 2.5YR 3/4 (dark reddish brown).

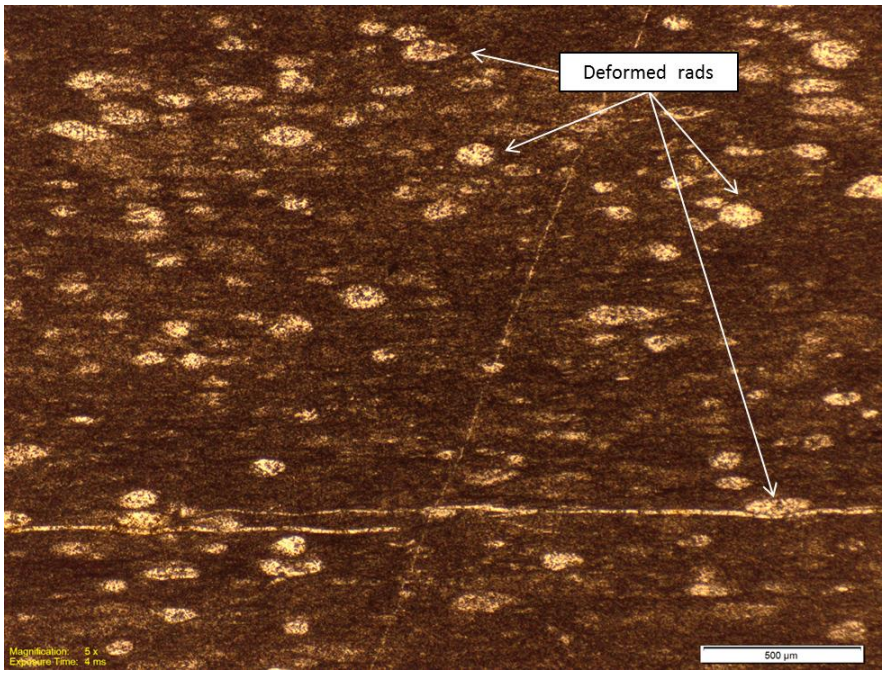

Figure 47 Sample B-13-16A thin section image showing deformed radiolaria and veinlets.

B-13-16A – Bedrock exposure mapped within the TKwph unit of Tabor *et al.* (2006). Foliated, fine grained, mostly uniformly dark red that lightens in color containing an uneven distribution of radiolaria remnants. Radiolaria are aligned along the plane of foliation and make up ~20-50% of the fabric. The section contains one relatively large quartz veinlet cross-cutting the fabric at ~45º, and multiple very fine quartz veinlets that mostly run parallel with the plane of foliation.

DISCUSSION

The thin sections from the samples collected by Cheney from various Puget Sound beaches have many differences from each other, but some general similarities are observable. Beach sample 14089 (Figs. 12 and 12) appears to be similar in hand sample to samples 14072 (Fig. 6), and B-25-15 (Fig. 20), but in thin section it differs drastically from all the samples. The radiolarian fossils present in sample 14089 are round and not distorted even though the sample does contain an abundance of white quartz veinlets that have been further altered and blended into the matrix. The larger veinlets also appear to contain the intact radiolarian remnants from the host rock. It is likely that the veinlets formed prior to compaction, because of the roundness of the radiolaria. This sample appears to be out of the confines of this study, does not share any similarities with any other rocks within the study, and is considered an outlier.

Samples 14086A (Fig. 9), 14086B (Fig. 11) in thin section appear to have experienced less deformation than the other beach samples and collected samples because of the presence of intact round radiolaria. Sample 14086A is composed of interbedded layers of clastic material and relatively undamaged round radiolarian remnants containing some silicified shell fragments and no veinlets present. The abundance of siliceous clasts found in this sample are not observed in any of the other beach samples, or collected samples, and may be the result of the introduction of volcanic ash or reworking event such as turbidity currents. The radiolaria found in sample 14086B are mostly slightly altered, but few unaltered round radiolarian fossils exhibiting their spiny skeletal structure do exist. The fossils are randomly dispersed within a dark matrix containing some clastic material and microcrystalline quartz swirls. Veinlets within this sample are sinuous and discontinuous and some that have been offset.
These two samples do not compare to any of the bedrock or river clast samples collected for this study, but there are some similarities when compared to sample SEG-207 (Fig. 14). In thin section sample SEG-207 (Fig. 15) contains a very similar matrix to samples 14086A (Fig. 9) and 14086B (Fig. 11), but contains a higher abundance of radiolaria than observed in sample 14086A, and less than 14086B. The radiolaria in SEG-207 vary in shape from equant to ellipsoidal as a result of a higher degree of deformation than found in either sample 14086A or 14086B. Sample SEG-207 also contains shell fragments and, clastic material as observed 14086A, and some quartz veinlets similar to those observed in 14086B.

The samples collected by the writer show little if any similarities to given beach samples collected by Cheney. Sample B-23-15 (Figs. 16-18) is the easternmost sample collected form Unit TKev (Fig. 5) closest to the tonalite pluton (unit Tst), and represents a foliated fabric unseen in any of the other samples in the study. This sample has experienced several generations of deformation, as evidenced by the multiple veinlet orientations and highly altered, almost unrecognizable radiolaria remnants. Because of its proximity to the tonalite pluton, sample B-23-15 probably experienced the highest temperature deformation of the collected samples. Sample B-25-15 (Figs. 19-21) was collected from a red boulder found on the Lake 22 trail (~1km from trailhead) and represents a moderately high degree of deformation in thin section. The remnants of radiolaria within this sample are all substantially deformed in the same direction to a higher degree than those found in the beach samples. This sample does contain distorted quartz veinlets that follow the foliation plane and show modest shearing. Sample B-25-15 is mapped within ice contact deposits (Fig. 4) and is considered to be glacial drift. These samples represent the greatest distortion found in this study.

Samples B-1-16A and B-1-16B (Figs. 35-40) were collected within the mapped unit TKwph, a phyllite containing locally abundant chert as described by Tabor *et al.* (2009). Sample B-1-16A contains highly distorted and reworked radiolarian remnants within a slightly crenulated texture. Sample B-1-16B contains distorted radiolaria remnants that are graded in abundance and no crenulated texture. Radiolaria found in sample B-1-16B are not as reworked and are clearer than the ones found in B-1-16A. Samples B-29-15 (Figs. 22-24) and B-30-15 (Figs. 25-26) were collected from mapped unit TKt which Tabor *et al.*

(2009) describe as a banded red and black recrystallized chert containing subordinate phyllitic argillite that is commonly highly sheared and mixed on all scales. The hand sample of B-30-15 (Fig. 25) shows more defined bedding than that in hand sample B-29-15 (Fig. 23). In thin section, both samples show relatively great distortion and shear (Figs. 24 and 26) judging from their elongate radiolaria and sheared veinlets.

Sample 14072 (Figs. 6 and 7) is considered the most promising beach sample in the study as it contains the most similarities with some of the collected samples. Sample B-31-15 (Fig. 27 and 28) is the most similar to sample 14072. Both samples contain both distorted ellipsoidal and undistorted round radiolarian remnants of similar size within a similar fine grained matrix. Both samples also contain offset white quartz veinlets, although they are less abundant and more faded into the matrix in sample B-31-15. Because both samples contain radiolaria of different shapes and offset veinlets, it could be possible that these samples have undergone multiple deformation events to varying degrees over time. Unfortunately sample B-31-15 was obtained from the bedload of a high alpine tributary to the head waters of Canyon Creek, not an *in situ* source. Samples B-12-16 and B-13-16A (Figs. 41-47) were collected from two separate bedrock sources that are relatively close together mapped within the TKwph unit. These samples differ from samples of the same mapped unit (B-1-16A and B-1-16B) in that they do not represent the same degree of deformation. Sample B-12-16 contains a darker matrix and more abundant radiolarian remnants deformed similarly to those in sample 14072. The veinlets found in B-12-16 are less abundant than observed in 14072, but are similar in size, and contain similar offset features. Sample B-13-16 is very similar to B-12-16, but appears slightly more deformed. The radiolarians in this sample are more stretched and are not as clear as those found in B-12-15.

Samples B-37-15A and B-37-15B (Figs. 29-34) where collected from extremely large red boulders within the North Fork Stillaguamish River channel and are similar to sample B-31-15 in thin section considering fabric color and veinlet distortion degree. Both samples (B-37-15A and B37-15B) contain abundant radiolarian remnants that are more distorted and faded than those found in sample 14072, although radiolaria found in sample B-37-15A (Fig. 31) are more equant than the round radiolaria found in sample B-37-15B (Fig. 34). These boulders are found in a reach of the river that contains an abnormally high abundance of similarly sized large boulders. Many red boulders of the same rock type are found here, but only the two largest accessible boulders where sampled. The boulder field extends upstream from the sampled boulders approximately 75m before the clast size drops drastically to more typical cobble sizes. Downstream the clast size degradation is more gradual and extends well over 300m. This region of large boulders may be remnants of a terminal moraine representing the furthest up valley extent of the Puget Lobe. Therefore, the boulders sampled could have been plucked from a bedrock source further east and deposited in their current location.

CONCLUSION

After petrographic analysis and comparison of the thin sections beach cobbles with the thin sections from collected bedrock and river clasts, it is apparent that some of the samples are similar. The most similar, 14072 and B-31-15, are still quite different. All of the *in situ* samples represent higher degrees of deformation than what is represented in the beach samples. Because of this difference it is not possible to definitely confirm or deny that the Canyon Creek unit of Vance (1957) is the exact origin of RC distributed throughout the Puget Lowland. What may be confirmed is that the depositional environment of the chert in the beach clasts and in the bedrock and river clasts is similar, but each group differs from the other diagenetically. The bedrock and river clasts samples show evidence of higher degrees of compaction, alteration, and in some cases metamorphism of originally clay-rich sediment to argillite and

phyllite. Just because this study cannot definitively confirm the Canyon Creek unit of Vance (1957) as a source for RC in the Puget Lowland, it is still plausible that it could be, given the similarities between the samples. It must further be noted that the material from the Fourth Lake Formation on Victoria Island, British Columbia (sample SEG-207) could also be a potential source for RC in Puget Sound based on similarities with beach samples (14086A, 14086B, and 14249B). Thin sections only represent a tiny portion of any sample, but it must be noted that even though the thin sections analyzed in this study do not show conclusive evidence for the determination of RC source, they show enough similarities to be very close to correct.

In order to determine whether or not the Canyon Creek is, in whole or in part, a source for RC within the Puget Lowland, a more intense sampling campaign of both beach cobbles and *in situ* bedrock must be undertaken. Sampling more beach cobbles would increase the sample diversity allowing better odds for a potential match to outcrops. Increased sampling on known locations of *in situ* rocks as well as a wider search for additional bedrock sources may also produce tighter similarities between samples or perhaps a match. In addition to increased sampling, other analytical methods could be undertaken to obtain additional data that may allow for further comparison. Geochemical analysis for trace elements may be able to determine if the samples of both regimes are of the same chemical makeup. Although the majority of samples collected represent various degrees of deformation, a radiolarian analysis may also be helpful given their abundance within the samples analyzed in this study.

Because this study is able to verify the Canyon Creek unit of Vance (1957) as plausible source of RC within the Puget Lowland a theory of RC transport can be proposed. It is widely accepted that during the Evans Creek Stade (~25 – 17.5 ka ^{14}C yr BP) of the Fraser Glaciation alpine glaciers from the Cascades and Olympic Mountains advanced into the Puget Lowland. During this time alpine glaciers would have mobilized and carried material (i.e. the Canyon Creek Unit of Vance [1957]) from its source in the mountains to lower depositional zones at or near the glacial termini. During the Vashon Stade (~17.5 – 12.5 ka ^{14}C yr BP) of the Fraser Glaciation, the Puget Lobe of the Cordilleran ice sheet would have remobilized the previously deposited alpine glacial deposits, essentially spreading the material throughout the Puget Lowland as it advanced toward the south and southwest.

REFERENCES

Boggs, S. Jr., 2009, Petrology of Sedimentary Rocks ed. 2: New York, Cambridge University Press, 600 p.

Calvert, S. E., 1983, Sedimentary geochemistry of silicon, *in* Aston, R. R., (ed.) Silicon Geochemistry and Biogeochemistry: Academic Press, London, p. 273-299.

Cheney, E.S., 2016, Overview of the Geology of Washington, *in* Cheney, E. S., (ed.) The Geology of Washington and Beyond; From Laurentia to Cascadia: Seattle and London, University of Washington Press, p. 18-20.

Cheney, E.S., Cowan, D.S., and Grupp, S.R., 2015, Some Geologic Highlights of the Whidbey and Guemes Islands in the Puget Lowland of Washington, Northwest Geological Society Field Guidebook Series, Fieldtrip Guidebook #407, Seattle, WA, Northwest Geological Society, 10 p.

Compton, R.R., 1972, Geology in the Field: New York, John Wiley & Sons, 397 p.

Dove, P. M., and Rimstidt, J. D., 1994, Silica-water interactions, *in* Heaney, P. J., Prewitt, C. T., and Gibbs, G. V., (eds.) Silica, Physical Behavior, Geochemistry and Materials Applications: Mineralogical Society of America Reviews in Mineralogy, no 29.

Easterbrook, D. J., 2016, Late Quaternary Glaciation of the Puget Lowland, North Cascades Range, and Columbia Plateau, Washington, *in* Cheney, E. S., (ed.), The Geology of Washington and Beyond; From Laurentia to Cascadia: Seattle and London, University of Washington Press, p. 257-286.

Gieskes, J. M., 1983, The chemistry of interstitial waters of deep sea sediments: Interpretations of deep sea drilling data, *in* Riley, J. P., and Chester, R., (eds.), Chemical Oceanography ver. 8, Academic Press, New York, p. 221-269.

Gunnarsson, I., and Arórsson, S., 2000, Amorphous silica solubility and the thermodynamic properties of H_4SiO_4 in the range of 0º to 350ºC at P_{sat}: Geochimica et Cosochimica Atca. no. 64, p. 2295-2307.

Massey, N. W. D., 1995, Geology and Mineral Resources of the Alberni – Nanaimo Lakes Sheet, Vancouver Island 92F/1W, 92F/2E, and 92F/7E, Provence of British Columbia Ministry of Energy, Mines, and Petroleum Resources, scale 1:50,000, 1 sheet, 132 p.

McCormack, D. H., and Troost, K. G., 2016, Quaternary Geology of Northwestern King County and Southwestern Snohomish County, Washington, *in* Cheney E. S., (ed.) The Geology of Washington and Beyond; From Laurentia to Cascadia: Seattle and London, University of Washington Press, p. 287-310.

Pessl, F., Jr., Dethier, D. P., Booth, D. B., and Minard, J. P., 1989, Surficial geologic map of the Port Townsend 30- by 60minute quadrangle, Puget Sound Region, Washington: U.S. Geological Survey Miscellaneous Investigations Series Map I-1198-F, 1 sheet, Scale 1:100,000, with 13 p. text.

Porter, S. C., and Swanson, T. W., 1998, Radiocarbon age constraints on rates of advance and retreat of the Puget lobe of the Cordilleran ice sheet during the last glaciation. Quaternary Research 50, no. 3, p. 205-213.

Rimstidt, J. D., 1997, Quartz solubility at low temperatures: Geochimica et Cosochimica Atca. no. 61, p. 2553-2558.

Tabor, R. W., 1994, Late Mesozoic and possible early Tertiary accretion in western Washington State: The Helena-Haystack mélange and Darrington-Devils Mountain fault zone, Geological Society of America Bulletin 106, no. 2, p. 217-232.

Tabor, R.W., Booth, D.B., Vance, J.A., and Ford, A.B., 2006, Database for the geologic map of the Sauk River 30-minute by 60-minute quadrangle, Washington (I-2592): U.S. Geological Survey, Data Series DS-188, scale 1:100,000, with 67 p. text.

Tabor, R. W., and Haugerud R. A., 2016, Geology of the North Cascades *in* Cheney E. S., (ed.) The Geology of Washington and Beyond; From Laurentia to Cascadia: Seattle and London, University of Washington Press, p. 131-154.

Tabor, R.W. and Haugerud, R.A., 1999, Geology of the North Cascades: A Mountain Mosaic: Mountaineers Books, Seattle, 144 p.

Vance, J. A., 1957, The Geology of the Sauk River Area in the Northern Cascades of Washington [PhD Thesis]: University of Washington, 313 p.

Vance, J.A., Walker, N.W., and Mattinson, J.M., 1986, U/Pb ages of early Cascade plutons in Washington State [abs.]: Geological Society of America Abstracts with Programs, v. 18, no. 2, p. 194.

Walther, J. V., 2005, Essentials in Geochemistry: Jones and Bartlett Publishers, Boston, 797 p.

Whetton, J. T., Carroll, P. R., Gower, H. D., Brown, E. H., and Pessl, F. Jr., 1988, Bedrock geologic map of the Port Townsend quadrangle, Washington: U.S. Geological Survey Miscellaneous Investigation Series Map I-1988-G, scale 1:100.000.

APPENDIX

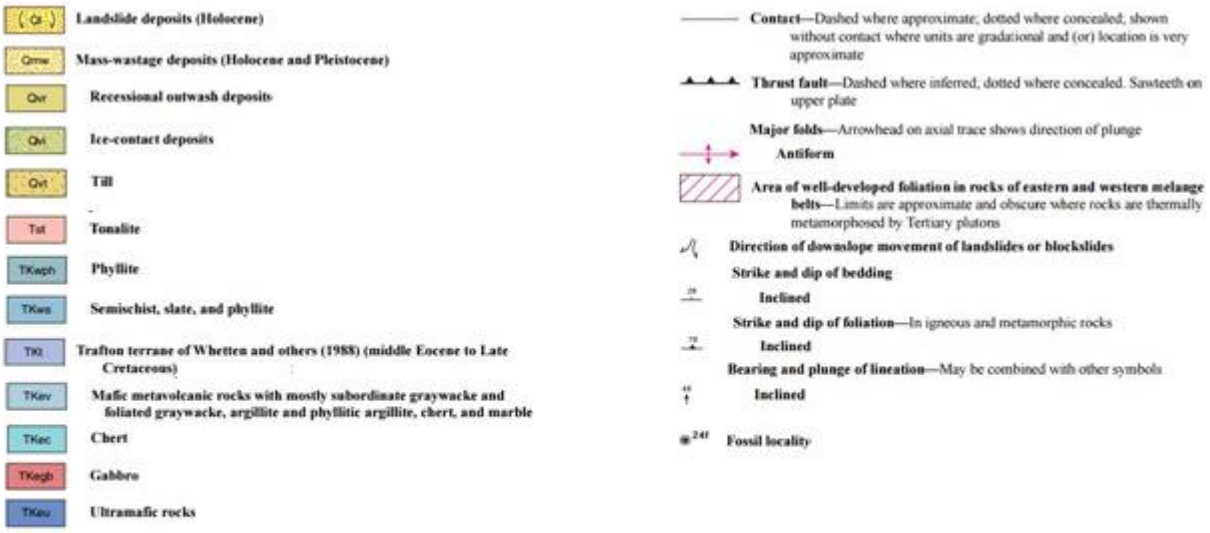

Figure 48 Map units and symbols pertaining to Figures 4, and 5, adapted from Tabor *et al*. (2006).

Table 1 Relevant rock units pertaining to Figures 4 and 5, adapted from Whetton *et al*. (1988) and Tabor *et al.* (2006).

Unit symbol	Unit Description
TKt	**Trafton terrane of Whetton *et al.* (1988) (middle Eocene to Late Cretaceous)** – Predominately greenstone and banded chert with subordinate greywacke and argillite. Commonly highly sheared and mixed on all scales, Chert is red and black, locally highly recrystallized. Minor diabase. Argillite locally phyllitic.
TKwph	**Phyllite -** Grey and brown to black phyllite, less abundant semischist, locally abundant chert and rare greenstone
TKev	**Mafic metavolcanic rocks with mostly subordinate greywacke, argillite and foliated greywacke, argillite and phyllitic argillite, chert, and marble** – Highly sheared and disrupted greenstone makes up from 20 to 50 percent of mélange and contains relict clinopyroxene (some titaniferous) and plagioclase in an altered matrix of chlorite, carbonate minerals, and pumpellyite.
TKec	**Chert** – Mostly white weathering, red or black ribbon chert and metachert making up to 20 to 80 percent of unit. Uniformly banded to complexly disrupted. Some chert as thin laminae in cherty argillite. Locally abundant greenstone, greywacke, and argillite.
Tst	**Tonalite** – Predominately uniform hornblende-biotite tonalite and granodiorite, medium-grained and hypidiomorphic granular. Locally rich in small hornblende diorite inclusions.

Table 2 Stratigraphy and chronology of the Fraser Glaciation (Adapted from Easterbrook, [2016])

FRASER GLACIATION	EVANS CREEK STADE	Evans Creek Drift ~25 – 17.5 ka ^{14}C yr BP • Advance of Alpine Glaciers into the Puget Lowland
	VASHON STADE	Vashon Drift ~ 17.5 – 12.5 ka ^{14}C yr BP • CIS 1800 m thick in the Fraser Lowland, 1000 m at Seattle, and extended to Olympia • Isostatic depression of the Puget Lowland under CIS • Melting and thinning of the CIS allows marine water into the lowland, floating the remaining ice sheet and causing the collapse of the CIS
	EVERSON INTERSTADE	Kulshan glaciomarine drift ~12.5 – 11.8 ka ^{14}C yr BP • Submergence of the lowland. Deposition of glaciomarine drift from floating ice from Whidbey island to southwest British Columbia • Deposition of Kulshan glaciomarine drift in the Fraser Lowland
		Deming sand ~11.8 ka yr ^{14}C BP • Emergence of the lowland. Relative sea level 6-12 m above present • Deposition of Deming fluvial and beach sand
		Bellingham glaciomarine drift ~11.7 ka ^{14}C yr BP • Submergence of the lowland to 180 m • Deposition of Bellingham glaciomarine drift in the Fraser Lowland • Shoreline cut at multiple levels in the Puget Lowland
	SUMAS STADE	Sumas ~11.4 -10 ka ^{14}C yr BP • Emergence of the lowland. Readvance of the CIS • Deposition of multiple moraines in the Fraser Lowland • Deposition of broad outwash plains in the Fraser Lowland • Large outburst floods in the Fraser Lowland

Table 3 Complete list of all location visited with short description.

Site #	GPS coordinate	Described location
B-23-15	48° 4'9.84"N, 121°38'35.47"W	Red bedrock exposure on Mtn Loop Hwy , refer to figure 23
B-25-15	48° 4'34.41"N, 121°45'3.20"W	Red boulders on Lake 22 Trail, refer to figure 19
B-27-15	48° 6'53.78"N, 121°57'49.25"W	Canyon Creek, red cobbles observed
B-28-15	48° 7'44.36"N, 121°50'39.01"W	Quarry, no red rock observed
B-29-15	48° 8'0.13"N, 121°50'42.18"W	Red bedrock in road bed, refer to figure 22
B-30-15	48° 8'2.22"N, 121°50'37.36"W	Red bedrock in road bed
B-31-15	48° 8'36.85"N, 121°46'28.67"W	Red cobble observed in stream bed on FS Rd-41
B-32-15	48° 8'38.44"N, 121°45'45.14"W	Stream, no red rock obs
B-33-15	48° 8'57.70"N, 121°44'53.56"W	Canyon Creek and FS Rd-41 Red cobbles obs, not abundant
B-34-15	48° 7'54.41"N, 121°50'28.21"W	Abandon Quarry, no red rock obs
B-35-15	48° 8'20.62"N, 121°49'46.56"W	Outcrop in roadbed, not red rocks obs
B-36-15	48° 4'19.09"N, 121°43'24.85"W	Downstream of B-37-15, meter sized red rocks obs
B-37-15	48° 4'13.08"N, 121°42'54.97"W	Zone of large red boulders in N Fork Stillaguamish River. Refer to fig. 34
B-38-15	48° 4'24.38"N, 121°41'37.03"W	Upstream of B-37-15 only one (17cm) red cobble obs
B-39-15	48° 4'25.14"N, 121°42'30.02"W	FS-Rd No red rocks obs
B-40-15	48° 4'22.84"N, 121°42'55.33"W	Wiley Creek Campground, small red cobbles obs
B-41-15	48° 6'9.90"N, 121°57'26.24"W	Below fish ladder in Granite Falls, small red pebble (<2cm) obs
B-42-15	48°14'25.55"N, 121°49'22.80"W	Boulder River waterfall, no red rock obs
B-43-15	48°15'39.17"N, 121°42'31.54"W	White Horse Trail, no red rock obs
B-44-15	48°12'23.90"N, 121°34'38.03"W	FS Rd-2060, no red rock obs
B-45-15	48°12'10.98"N, 121°34'33.56"W	FS Rd-2060, no red rock obs
B-46-15	48°11'29.47"N, 121°34'32.56"W	FS Rd-2060, no red rock obs
B-47-15	48°10'27.26"N, 121°28'22.84"W	While Creek boat launch, Sauk River, no red rocks obs
B-48-15	48° 4'4.91"N, 121°24'29.88"W	S Fork Sauk River and Mtn Loop Hwy, no red rock obs
B-49-15	48° 7'1.49"N, 121°31'20.53"W	FS Rd-4060, no red rock obs
B-50-15	48° 6'28.04"N, 121°34'20.60"W	FS Rd-4052 no red rock obs
B-51-15	48° 4'23.81"N, 121°41'39.12"W	Upstream limit of large red boulders in S Fork Stillaguamish River
B-52-15	48° 4'22.55"N, 121°41'20.22"W	Esswine Campground, one red boulder (~.5m) obs

B-1-16	48° 6'30.24"N, 121°44'21.62"W	End of FS Rd-4111, red bedrock exposure, refer to figure 35
B-2-16	47°46'16.72"N, 121°29'18.71"W	Skykomish River, Baring, WA, no red rock obs
B-3-16	47°42'35.60"N, 121°21'46.84"W	Skykomish River, Skykomish, WA, no red rocks obs
B-4-16	48°12'17.35"N, 122° 7'40.94"W	Confluence N and S Forks Stillaguamish River, few red cobbles obs
B-5-16	48°16'2.28"N, 122° 0'43.85"W	N Fork Stillaguamish River and Hwy 530 bridge, few red cobble obs
B-6-16	48° 4'30.14"N, 121°42'32.47"W	~200m upstream of B-37-15 one red and white boulder obs
B-7-16	48° 4'14.34"N, 121°39'14.44"W	Red Bridge Campground, no red rock obs
B-8-16	48° 4'11.96"N, 121°40'44.11"W	Boardman Creek Campground, only small red cobble obs
B-9-16	48° 4'46.63"N, 121°44'28.32"W	West of Wiley Creek Campground, red boulder obs
B-10-16	48° 5'50.75"N, 121°58'16.46"W	Confluence of Canyon Creek and NFSR, small red cobbles obs
B-11-16	48°10'11.75"N, 121°41'16.55"W	Three Fingers lookout, no red rock obs
B-12-16	48° 7'36.52"N, 121°46'29.86"W	Red bedrock exposure, refer to figure 43
B-13-16	48° 7'43.50"N, 121°47'5.42"W	Red bedrock exposure, refer to figure 46